Materials Today Communications 41 (2024) 111042

Contents lists available at ScienceDirect

Materials Today Communications

journal homepage: www.elsevier.com/locate/mtcomm

Self-expanding Nitinol stents for endovascular peripheral applications: A review

Farzaneh Hoseini [a], Alberto Bellelli [a], Luke Mizzi [a], Felice Pecoraro [b,c], Andrea Spaggiari [a,*]

[a] Department of Science and Methods for Engineering, University of Modena and Reggio Emilia, Reggio Emilia, Italy
[b] Vascular Surgery Unit - AOUP Policlinico 'P. Giaccone', Palermo, Italy
[c] Department of Precision Medicine in Medical, Surgical, and Critical Care (Me. Pre.C.C.) – University of Palermo, Italy

ARTICLE INFO

Keywords:
Peripheral stent
Nitinol
Self-expanding stent
Arterial and venous stent
Biomedical engineering

ABSTRACT

Peripheral arterial diseases affect a significant portion of the global population, fostering research to find innovative and effective solutions to improve people's life. A primary focus for researchers and manufacturers is the continuous improvement of the most important, non-surgical treatment for this pathology, the endovascular stent. This device is the main feature enabling a lifesaving technique: the percutaneous vascular interventions. Stents are vital for restoring blood flow and enhancing long-term vessel patency, they are available in various materials, shapes and typologies. Recent advancements in stent design, particularly through additive manufacturing, create new opportunities for optimizing the device performance and possibly opening new areas of intervention. This review provides a detailed quantitative analysis on the most widely used category of devices: self-expanding stents made of Nitinol, a nickel-titanium alloy that shows a superelastic behavior. A set of figures of merit related to stent design are described and analyzed, with a focus on the influence of geometry on mechanical performance. Additionally, a comprehensive comparative analysis of the commercial stents evaluates the geometry and performance of many commercial solutions, including both arterial and venous types. This analysis offers quantitative tools to assist surgeons and designers in selecting the most important features of a stent with respect to its main application. To conclude this work, an overview of future manufacturing possibilities is provided mainly focusing on the additive manufacturing technology. The freedom of shape given by this method opens up new paths in terms of global shapes, strut geometry and sizes, revealing new avenues which point strongly towards ad-hoc and specifically patient-customized stent design.

1. Introduction

Atherosclerosis is the hardening and narrowing of blood vessels caused by the accumulation of plaque or lipid deposits lining the vessels over time, causing vascular occlusion, and affecting the blood flow. Severe atherosclerosis could lead to diseases like coronary artery disease, cardiovascular disease, peripheral artery disease (PAD), and other cardiovascular pathologies. Historically, traditional surgical operations have been utilized to address severe cases of atherosclerosis. However, in recent years, percutaneous vascular intervention (PVI) has emerged as one of the most effective alternative treatments [1]. Unlike traditional open surgery, PVI is a minimally invasive treatment in which a catheter with a balloon or stent is inserted into a stenosed or occluded vessel to open it up and restore the cardiovascular circulation which has been clogged by atherosclerosis. Percutaneous transluminal angioplasty (PTA), venoplasty, and stenting are different types of PVI techniques. PTA involves inserting and inflating a balloon within the narrowed artery to compress the plaque away and widen the vessel lumen, while venoplasty extends this concept to the venous system, addressing stenoses/occlusions and restoring venous patency by using a similar balloon dilation technique in veins rather than arteries [2]. Stenting, on the other hand, involves placing a stent in the stenosed/occluded vessel permanently to provide structural support and prevent the vessel from recoiling and re-narrowing. A stent is a tiny tubular structure, which is in most cases made of metal, to support and maintain the patency of narrowed or blocked vessels.

Compared to traditional open surgery methods, PVI stenting offers several clinical advantages. By eliminating the need for conventional open surgery, PVI stenting minimizes patient trauma, operation time, hospital stays and convalescence. Beyond its clinical implications, PVI stenting is advantageous on the economic side for both healthcare

* Corresponding author.
E-mail address: andrea.spaggiari@unimore.it (A. Spaggiari).

https://doi.org/10.1016/j.mtcomm.2024.111042
Received 8 July 2024; Received in revised form 23 October 2024; Accepted 17 November 2024
Available online 22 November 2024

Abbreviations

Medical-related

BDS	Biodegradable Stent
BMS	Bare Metal Stent
BRS	Bioresorbable Stent
BX	Balloon-Expandable
DES	Drug-Eluting Stent
FPA	Femoro-Popliteal district Arteries
ISR	In-Stent Restenosis
PAD	Peripheral Artery Disease
PTA	Percutaneous Transluminal Angioplasty
PVI	Percutaneous Vascular Intervention
SFA	Superficial Femoral Artery
ST	Stent Thrombosis
SX	Self-Expanding
WSS	Wall Shear Stress

Engineering-related

AM	Additive Manufacturing
COF	Chronic Outward Force
CR	Crush Resistance
LB-PBF	Laser-Based Powder Bed Fusion
OS	Oversizing
RRF	Radial Resistive Force
SME	Shape Memory Effect

systems and patients, as it decreases the need for prolonged hospitalization, post-operative care, and rehabilitation expenses. Additionally, PVI stenting provides benefits on the social side by offering patients faster recovery times and lowering re-hospitalization chances, allowing them to return to their daily activities sooner.

PAD presents a significant economic burden; the annual costs on hospitalization alone in the U.S. exceeding $21 billion [3]. As stated previously, stenting has emerged as a promising solution in endovascular peripheral applications due to their remarkable mechanical properties and potential clinical benefits. However, the success of stenting relies on a comprehensive understanding of key factors influencing stent performance. This review aims to bridge the gap between stent design and clinical application by providing information on key fac]ors such as design parameters and mechanical characteristics of the stent and their link to stent performance. This information will assist both the designer and the clinician in selecting the most suitable characteristic based on their individual requirements, thereby enhancing patient outcomes, and reducing the financial impact associated with PAD by optimizing stent selection.

1.1. Evolution of stents

The pioneer researcher in the field of stenting was Dr. Charles Theodore Dotter, a radiologist who was the first to describe angioplasty, in 1964, together with his trainee Dr. Melvin P. Judkins. He designed and developed a stainless steel “coil spring graft” successfully placed in the femoral artery of a dog [4]. He also developed Nitinol (NiTi) coil wire stents [5] that led future research on stenting [6]. In 1986 doctors U. Sigwart and J. Puel placed the first stainless steel stent into the stenosed lesion of a man, immediately following balloon angioplasty [7–9]. After this first intervention, the use of stents grew exponentially and there has been continuous improvement in the design and materials of the stents since then. Unfortunately, the first generation of bare metal stents (BMSs) showed in-stent restenosis (ISR) rates up to 20 %, leading to necessary re-intervention [10]. ISR is a gradual re-narrowing of a stented vessel segment that can occur few months after stent placement [11]. Adverse effects were not only caused by the stent itself, but also by its malapposition and, in general, by the deployment methods [10,12]. Nevertheless, research on nondegradable BMSs rapidly led to the development of better performing stents characterized by good processability, mechanical properties, and economical efficiency which are currently in use for various treatment of cardiovascular diseases [12]. A decade later, the first drug-eluting stents (DESs) were used, improving clinical outcomes by minimizing ISR rates down to 4 % [10]. DESs, like BMSs have the base platform made of stainless steel, CoCr alloys, NiTi alloys, or other biocompatible alloys, but they also provide drug delivery (e.g. paclitaxel, everolimus) through a coating technology (polymer--controlled or polymer-free). Localized drug delivery was an important improvement in the development of better-performing stents, resulting in a decrease in ISR rates, however, the problem of stent thrombosis (ST) [9] remained unsolved.

Stent thrombosis is more common in perioperative peripheral arterial disease patients, especially those with chronic total occlusion lesions. Factors such as stent type, loss of collaterals, and edge restenosis contribute to stent thrombosis. Additionally, complex lesion characteristics, dual antiplatelet therapy duration, and stent fractures play a role in stent thrombosis [13]. Non-stented thrombosis rates affecting the femoro-polpliteal district vary with different angioplasty methods. Histopathological studies reveal collagen deposition, intramural calcification, and thrombotic material in chronic total occlusion lesions, which affect stent expansion. Short dual antiplatelet therapy duration may significantly contribute to stent thrombosis. Disease location, especially in superficial femoral artery stents, influences stent thrombosis risk [14,15]. Distal stent locations contribute to worse long-term outcomes due to contiguous popliteal and infrapopliteal disease [16,17].

Ideally, a stent, after being implanted and having performed its function for the expected timeframe, would disappear. Although this is utopian, considerable research has been carried out on the development of biodegradable/bioresorbable stents (BDSs/BRSs), both with a polymeric or metallic platform. The degradable polymers include polylactic acid (PLA), poly-L-lactic acid (PLLA), polycaprolactone (PCL), racemic polylactic acid (PDLLA) and many others. The degradable alloys include magnesium, zinc and iron alloys [8]. The use of BDSs would bring many clinical benefits, such as avoiding adverse events associated with the presence of the stent in the vessel, recovering the unimpeded vasomotion [18] of vessels (which was due to the presence of a “foreign body” like a stent), and the possibility for the patient to undergo MRI (magnetic resonance imaging) without concerns [19]. Unfortunately, initially developed BDSs had strut thicknesses much higher than their nondegradable counterparts to compensate for their weaker mechanical properties [10], especially due to the low elastic modulus of the biodegradable material. BDSs are still considered a promising development, but their associated drawbacks mean that there is still need for further investigations before they can be widely utilized [9].

1.2. Classification of stents

Stents can be classified based on different factors, such as the stent’s topology, material selection and deployment method. Here, we classified them based on the material properties and subsequent insertion/deployment method, which can be either self-expanding (SX) or balloon-expandable (BX).

Balloon-expandable and self-expanding stents. In BX stents, the stent is mounted on a balloon-tipped catheter and deployed at the plaque site by means of a guide-wire. When the stent is in place, the balloon is inflated, causing the stent to expand and apply radial pressure against the vessel walls. This breaks the plaque, which is often calcified, recovering the vessel patency, and providing structural support. After

deployment, the balloon is deflated and removed, leaving the stent in place due to plasticization of the material (Fig. 1a). Conversely, SX stents are designed to expand on their own once deployed due to their inherent material properties. These stents are crimped onto a delivery system inside a sheath and deployed in position. Upon release from the delivery system, the sheath is removed, and the stent expands until it reaches the vessel wall, exerting outward pressure to keep the vessel open. The expansion is due to the superelastic recovery of the NiTi alloy from which the stent is made, as elaborated upon in the next section. Like BX stents, SX stents are left in place permanently to provide long-term support, prevent vessel recoil, and maintain blood flow (Fig. 1b).

It must be noted that angioplasty or other vessel preparation technique can be performed before inserting a SX stent [20] for several reasons, including preparing the lesion site by dilating the narrowed artery, facilitating stent positioning and deployment, debulking atherosclerotic plaque to create space for stent placement, and reducing the risk of complications. This preparatory step is particularly crucial in cases of calcified lesions or tortuous vessels to ease stent delivery and ensure optimal stent function. More often SX stents require post dilation balloon angioplasty to reach full expansion and proper arterial wall apposition. SX stents exhibit continued expansion over several days until they reach their maximum diameter, typically occurring within a few weeks following implantation [7] as opposed to BX stents, where the maximum diameter is achieved immediately upon implantation.

During the manufacturing process, BX stents are produced in a crimped state and then expanded to the diameter of the vessel by inflating a balloon, resulting in the stent being plastically deformed. Therefore, BX stents must be able to withstand plastic deformation to maintain the required size after deployment [21,22]. On the other hand, SX stents are typically designed with a slightly larger diameter than the vessel in which they will be deployed, therefore, they must possess sufficient elasticity to be crimped into the smaller delivery system before expanding in the desired position [22]. The lower elastic modulus of SX stents, compared to BX stents, makes them more compliant and therefore easier to insert, thus reducing the risk of stent dislodgement and migration [21,23].

BX stents have limited radial compliance compared to SX stents, making them more susceptible to permanent deformation when exposed to external forces. This limitation affects their performance in arteries like the femoro-popliteal district ones, which experience significant deformation (torsion and bending) during daily activities. SX stents are better suited for dynamic arteries with large biomechanical deformation such as these [24]. SX stents can also better adapt to artery's shape and diameter, making the deployment easier and minimizing trauma during implantation [25]. BX stents show less recoil in comparison to their SX counterparts when placed in calcified lesions, hence they are still preferred for renal and coronary stenting [21].

All this indicates that SX and BX stents have important differences for clinical and mechanical purposes and their suitability for insertion is primarily determined by the type of the vascular system in question. In this review, we will focus primarily on SX stents and their applications in venous and arterial vessels.

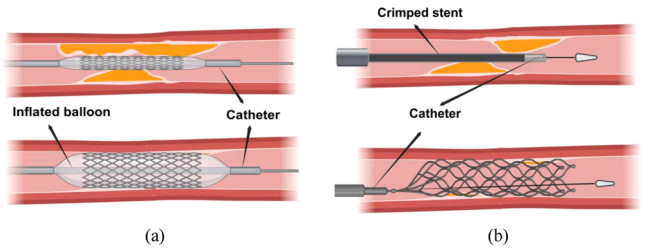

Fig. 1. Two deployment methods of stents: (a) balloon-expandable stents, (b) self-expanding stents.

1.3. Available materials for stents

The selection of materials for stent fabrication is a critical aspect, which involves several key factors to ensure optimal performance and patient safety. The primary concern is the biocompatibility of the stent, ensuring that it does not induce any adverse reactions when deployed into the patient's body. Furthermore, the stent material must have radiopacity, allowing for easy detection under fluoroscopic imaging to ensure the stent is positioned accurately during deployment. Moreover, it is crucial to select a stent material with excellent corrosion resistance to avoid corrosion, as this significantly impacts the long-term durability and performance of the stent [26].

In addition to the previously mentioned characteristics, stents require specific mechanical properties as a result of a balance between stiffness (required to sustain dilation and resisting elastic recoil of the vessel) and compliance (to accommodate bending during the deployment phase and during the body movement). Fig. 2a shows a typical stress-strain curve illustrating the behavior of ceramics, metals, and polymers. Unlike ceramics, which has a low fracture toughness and lack plasticity, and polymers, which struggle to achieve sufficient strength and stiffness, metals are an excellent choice for manufacturing stents due to their natural balance of elasticity and rigidity compared to other materials [27]. Generally, the metals often used in stent manufacturing include 316 L stainless steel (316 L SS), cobalt-chromium (CoCr), Nitinol (NiTi), titanium (Ti), magnesium (Mg) alloys, pure iron (Fe), platinum-iridium (PtIr) alloy and tantalum (Ta) [12,22].

The characteristics of materials required for stents vary depending on the application. NiTi is one of the most effective materials for SX stents [26,28]. In fact, a SX stent must undergo large deformation and have quite low elastic modulus to maintain its compliance, allowing it to be crimped inside a sleeve for delivery and expanded after deployment [29,30]. On the contrary, BX stents must have high modulus of elasticity for minimum recoil and possess high strength and the ability to work also slightly beyond the elastic region [22,26], making the stainless steel an appropriate materials for this kind of stents [26].

Fig. 2b shows the static stress-strain curve of stainless steel and NiTi, where it can be seen that, thanks to its superelastic behavior, NiTi could reach large deformations (more than 8 %) [31], and yet being capable of recovering its initial shape. As this work is intended to focus its attention on NiTi SX stents, an insight on NiTi is provided in the next paragraph.

NiTi has two main solid phases with distinct features and characteristics; austenitic phase, also called parent phase, which is stable under low stress and high temperature, and martensitic phase, also called daughter phase which is stable under high stress and low temperature [33]. In addition, the martensitic phase is divided into two forms: twinned and detwinned. Detwinned martensite is a state in which the martensite crystals have undergone a process that removes the twin boundaries, resulting in a more stable microstructure. Twinned martensite, on the other hand, has twin boundaries making the material

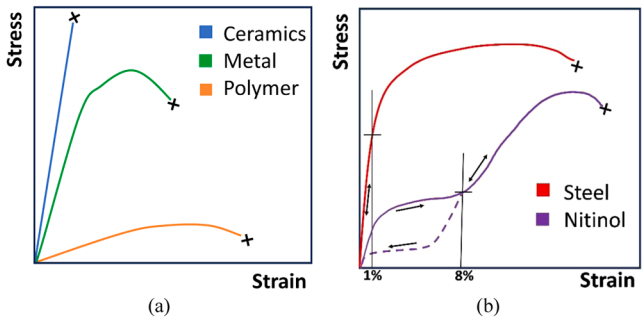

Fig. 2. (a) Qualitative stress-strain curves of metals, ceramics, and polymers, adapted from [27], (b) stress-strain curve of stainless steel and NiTi, adapted from [32].

less stable. The detwinned martensite is stable at high-stress state regardless of temperature, while twinned martensite is stable at both low-stress and low temperatures, as shown in Fig. 3 [34]. NiTi satisfies the requirements for medical applications, due to its excellent biocompatibility, mechanical properties, and corrosion resistance. However, it is important to note that Nitinol's inherent radiopacity is lower than that of traditional stainless steel stents, which can hinder clear visibility under imaging techniques such as fluoroscopic and X-ray imaging [35]. This visibility is essential for accurate stent placement and effective post-procedure monitoring. To address this limitation, radiopaque markers made of high density materials (platinum, gold [36] and tantalum [37]) are inserted at key points of the stent and significantly enhance visibility during imaging. This approach offers practical solutions to enhance the stent's visibility without compromising its mechanical properties. NiTi also exhibits remarkable properties such as shape memory effect (SME), and superelasticity attributed to its peculiar crystal structure and phase transformation between austenite and martensite [38]. The solid-state transformation from austenite to martensite occurs almost instantly by rapid cooling or by inducing stress. Fig. 3 demonstrates the SME and superelasticity characteristics of NiTi, highlighting its remarkable mechanical properties and functional capabilities.

When a sufficiently large mechanical stress is applied to the NiTi in its austenite phase, as shown in point 1 in Fig. 3, it undergoes a phase transformation to the detwinned martensite phase. In this phase, NiTi can tolerate much higher levels of strain than other materials, without experiencing permanent deformation. When the stress is released, point 2 in Fig. 3, NiTi spontaneously reverts to its original austenite phase and shape. This ability to undergo large recoverable deformations is what grants NiTi its superelasticity. Unlike typical metal alloys that have recoverable deformability below 1 %, elastic recovery of NiTi can reach up to 8 % strain [39–41]. It is important to note that the superelastic mechanical properties of NiTi are only evident within the temperature range between the austenite finish and detwinned martensite deformation temperatures ($A_f < T < M_d$) [42]. For the case of SX stent design, it is possible to benefit from the superelasticity of NiTi as the performance of a SX stent is dependent on the ability of the material to store elastic energy whilst it is constrained in the delivery system, making it an ideal choice for manufacturing this kind of stents [28]. Most of the NiTi stents can be crushed until they are almost completely flat and yet return to their original shape without any permanent deformation. This feature is especially important in superficial vessels like the carotid artery that are vulnerable to external crushing [28].

The transition from point 1 to point 2 in Fig. 3, depicts the loading process, in which the stent is crimped into the delivery system. The transition from point 2 back to point 1 represents the process once the stent being released from the delivery system, showing its inclination to return to its original shape and phase. The shape memory properties of

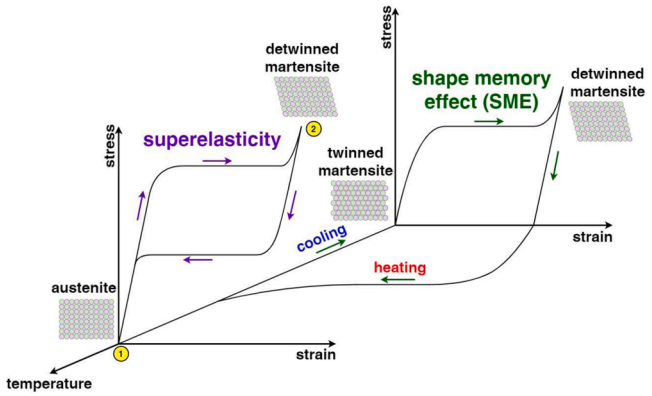

Fig. 3. Shape memory effect and superelasticity of NiTi, adapted from [38].

the NiTi are not utilized in stenting applications, since the transition temperatures (which are dependent on the stoichiometric element ratio) ensure that the material never transitions to the twinned martensitic phase at body temperature.

In most cases, after the insertion of SX stents, additional angioplasty procedures are also performed to help the stent better performance and efficiency [21,43] and this procedure increase the complexity of the force displacement path of a NiTi stent during deployment. For instance, based on the work of T.W. Duerig and M. Wholey [21], Fig. 4 shows a schematic to clarify this point by showing normalized radial forces (N/mm) on the stent and on the vessel, with respect to their diameters (mm), in three phases of stent deployment. The dashed blue line depicts the initial crimping of the stent, from a completely uncrimped stent (maximum diameter, no radial force on it (point **a** in the Fig. 4), to a crimped state (minimum diameter, maximum radial force on it, point **b** in the Fig. 4). Upon release from the sheath, the stent expands until it encounters the inner wall of the vessel at point **c**. From this point the force on the vessel increases until the stent and the vessel find an equilibrium diameter and stress (point **d** in the Fig. 4). Further expansion is then achieved through balloon angioplasty, extending the stent to point **e**, which in turn causes the vessel to expand to the same diameter (point **e'**). Following balloon deflation, compressive force from the vessel is exerted on the stent, causing it to recoil to the diameter at point **f**. This marks the final equilibrium in stress and diameter between the stent and the vessel. It should be noted that the stiffness during the loading of the stent, k_l (initial crimping phase and last recoiling phase after angioplasty) is larger than the stiffness during the unloading, k_u, of the stent, according to the hysteresis cycle due to the superelastic nature of the material.

1.4. Stent manufacturing techniques

Stents are not of simple manufacture; their strut thickness is of the order of magnitude of hundreds of microns; therefore, they need careful manufacturing and strict tolerances. Moreover, being medical devices, they need to be compliant with strict guidelines and rules, for example in Europe they need to have the CE (Conformité Européenne) mark and in the United States the FDA (Food and Drug Administration) approval is required. The manufacturing techniques that are commonly used are the braiding technique, microinjection molding, laser cutting, and recently additive manufacturing [9], some examples of which are shown in Fig. 5. Generally, stents are not immediately usable after the manufacturing process because their surface quality must be improved to increase the stent's fatigue life, to grant its biocompatibility, and to diminish abrasion problems that could cause vessel injuries; therefore, stents usually undergo a series of post-processing steps after fabrication.

1.5. Braiding technique

Fig. 5a shows an image extracted from a patent for the braiding technique of stents [44]. The braiding technique consists of winding wires (for example six interwoven NiTi wires in the case of Abbott Supera [47]) around the carrier, and then the wires are woven along the axis of rotation of the stent in order to build it [7,9]. Braided stents have a simple shape, very high torsional stiffness and do not buckle even under high axial compression [48]. However, their main drawback is a low radial stiffness [7].

1.6. Laser cutting technique

It is not possible to manufacture stents with conventional CNC (Computer Numerical Control) machining techniques, due to the high wear of the tool, poor dimensional accuracy and incompatibility with the intrinsic material properties of NiTi. Therefore, the laser cutting technique is currently the most widely used method for stent fabrication. The feedstock is a tubular workpiece of the desired material (for

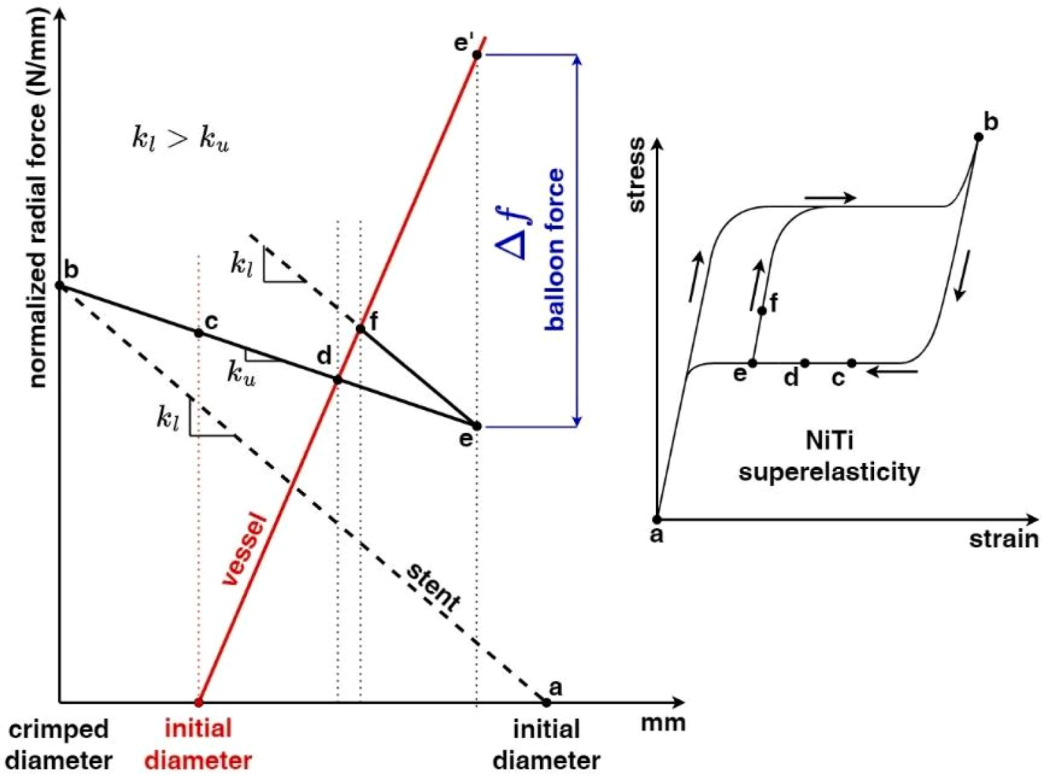

Path	Force-displacement diagram	Stress-strain diagram
a →b	Minimum stent diameter, max force reached with k_l stiffness	First loading phase, max stress and strain
b → c	Stent deployment, force decrease with k_u stiffness, onset of vessel impingement	Unloading following lower stiffness branch
c →d	Stent and vessel reach a first equilibrium point in **d** (before balloon angioplasty)	
d → e / e'	Balloon inflation, vessel expansion to point **e'**, stent expansion to point **e**	
e / e' → f	Balloon deflation, vessel and stent reach last equilibrium point	Second loading phase due to vessel elastic spring back

Fig. 4. Schematic (adapted from [21]) of radial force exerted by a NiTi SX stent when deployed in a vessel with subsequent angioplasty as a function of the diametral dimension (left) and schematic stress-strain curve of superelastic NiTi (right).

example, NiTi) with the desired diameter and thickness. A high-energy-density laser beam is focused on the surface of the workpiece and the material vaporizes leaving the desired stent mesh. The remaining material is then blown away by a pressurized air flow [7,9,49]. As a result, the cross section of the ligaments is roughly rectangular. This type of cross section has been reported to possibly promote turbulences in blood flow, which could lead to restenosis and late stent thrombosis [50]. After being laser cut, the NiTi microtubes are heat-treated and chemically etched to obtain the desired mechanical properties and surface finish [51].

1.7. Additive manufacturing techniques

Additive manufacturing (AM) of stents is an area of growing research that has the potential to lead to substantial improvements in patient outcomes due to its ability to rapidly develop custom stents. Laser beam technology has developed to the point that today laser beams are very small (typically 20–80 μm); therefore, they can provide not only the means for developing stents through subtractive manufacturing, but also AM through laser powder bed fusion [49]. Powder bed fusion (PBF) is defined by ISO/ASTM 52900:2021 standard and is an AM technique that uses either laser or electron beams to selectively melt or fuse powder particles on a powder bed in a layer-by-layer manner. Other PBF techniques such as electron beam powder bed fusion (EB-PBF) are unsuited for manufacturing vascular stents due to the larger spot size of the electron beams (about 100 μm) [52]. Therefore, nowadays only laser-based powder bed fusion (LB-PBF), sometimes also called selective laser melting, is a viable manufacturing technique for NiTi stents.

For what concerns the mechanical properties of additive-manufactured NiTi devices, they have been compared with the mechanical properties of NiTi devices obtained with traditional manufacturing techniques (e.g. laser cut) in several studies; for example, a work from Meier et al. [53] shows that both AM NiTi and conventional NiTi materials show a similar functional behavior during thermo-mechanical cycling, whereas fracture strength and fracture strains of AM NiTi are slightly lower. This highlights that AM is a promising manufacturing method for NiTi alloys. Another difference regards the surface finish of AM NiTi parts compared to conventional NiTi parts.

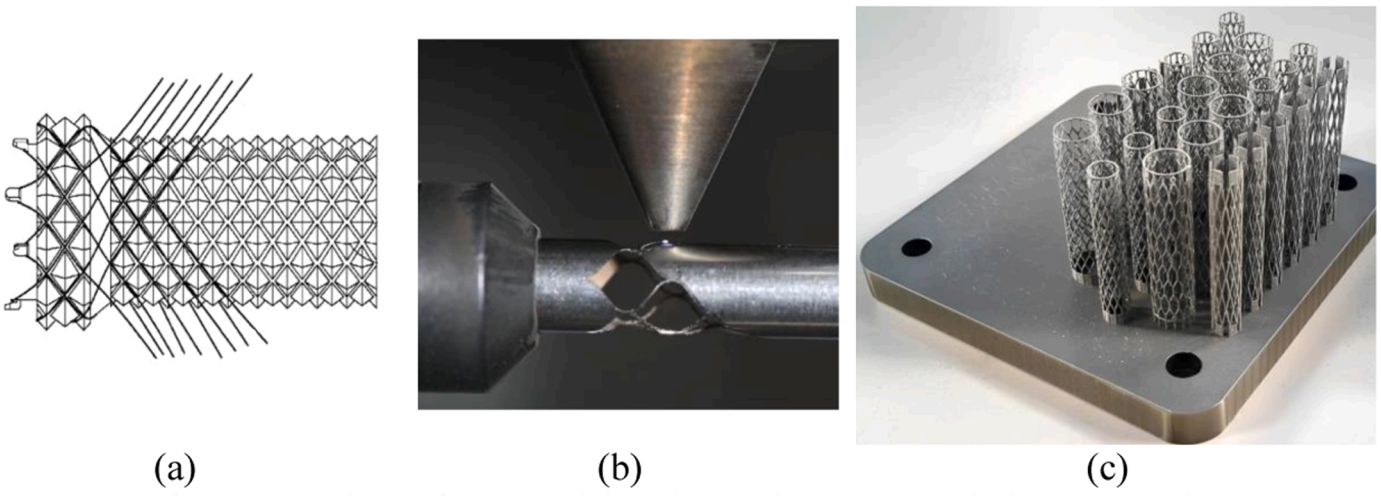

Fig. 5. Manufacturing technique of stents: (a) braiding technique [44], (b) laser-cut technique [45], and (c) additive manufacturing (AM) [46].

The most important advantage of applying AM to stent manufacture is the ability to produce fully customizable stents and, in general, medical devices based on patient-specific 3D models. These stents would have a variable geometry that is consistent with the anatomy of the patient. This design flexibility has also been demonstrated with the production of bifurcated geometries [54]. Another advantage of AM of stents is that the production is not dependent or limited by the availability of suitable commercially available tubes for laser cutting. For the latter method, when the available tube diameters do not perfectly match the ideal diameter needed for the anatomy of a specific patient, the surgeons select a stent with a diameter slightly larger than necessary to ensure proper fitting, which could lead to negative consequences such as irritation of the vascular wall and possible inflammatory response due to stent oversize [55]. Furthermore, one last advantage not to be overlooked in utilizing the LB-PBF techniques, is waste minimization during production, compared to laser cutting.

However, there are also some significant limitations in the manufacture of AM stents. A main issue regards the low surface quality of the as-built surfaces, especially since the required strut thicknesses of NiTi stents are very small, in the order of 100–500 μm, which is comparable to the size of the powder particles (10–60 μm) and the laser beam. This requires careful control of the energy release but also the scan vector accuracy [49,54]. Many studies point out that only the energy level is not sensitive enough to predict the printing quality [50]. In addition, shape-memory and superelasticity properties are highly dependent on the powder composition and process settings. Any slight changes in the nickel content due to the laser melting during the process in the composition can change the transformation temperatures and, subsequently, the superelastic behavior of the AM stents [56]. This further increases the difficulty of parameter optimization in the fabrication of thin NiTi structures through this method. The high-intensity laser beam could lead to increased porosity, significant residual stress, and high surface roughness [52]. A balance between the porosity and the transition temperature control is hard to achieve by controlling the laser process parameters, hence, consecutive heat treatments and surface finishing operations may be applied to modify the microstructure as-built and improve the mechanical properties of AM stents [51]. To improve the surface quality of LB-PBF stents, chemical etching must be performed. This process also lowers the strut thickness, improving the stent performance [51,56]. This technique and other surface modifications, such as coating, passivation, laser polishing [57] and electropolishing, can also be advantageous in overcoming the potential issue of nickel release into the bloodstream in the human body, which is a fundamental issue to avoid in order to guarantee the biocompatibility of the stent [56,58,59]. Another important aspect to be considered for the AM of NiTi stents is that additive manufactured devices often present anisotropic mechanical properties due to the intrinsic manufacturing techniques adopted [60]. More precisely, there could be a different mechanical behavior of the stent due to the direction of printed layers. Building direction and scanning pathway are shown to greatly influence the behavior of additive-manufactured devices: M. Somireddy and A. Czekanski [61], showed that building orientation (edge, flat or upright) of additive-manufactured composite structures significantly influences the final properties of the structure, tested through flexural loading, while S. Dadbakhsh et al. [62], showed how building direction, scanning direction and scanning speed influence the compression behavior and shape memory response of selective laser melted NiTi specimens. The anisotropy of a device, often considered a negative aspect, could be exploited to modify the mechanical behavior of a stent in one direction compared to the others, but these considerations are beyond the scope of this review article. Future investigations in this sense will be necessary in the search for the ideal stent for the specific need. Furthermore, the design phase also needs to be considered when utilizing LB-PBF to produce NiTi stents. The stent design should avoid large overhangs to minimize supports during printing, and in addition, removing the support structure would affect the surface roughness of the final product [52,54–56]. Despite these limitations, AM opens up new avenues in terms of customization of the devices, which could be tailored to the patient's vessels in combination with precise preoperative assessment (e.g. CT scan or MR).

To summarize, vascular stents are hollow structures used to maintain or restore vessels' patency, either for coronary or endovascular applications. They can be bare metal or drug-eluting, self-expanding or balloon-expandable, they are typically made of metals (stainless steel, CoCr, NiTi) and manufactured mostly through laser cutting of tubes and braiding of wires with AM technology which is rapidly growing as a viable way [63]. This work investigates a specific category: self-expanding Nitinol stents for endovascular peripheral applications, since they cover an important portion of the global market of stents, and they are one of the best candidates for AM applications.

In the next part of this review, an overview of commercial-available NiTi SX stents is provided by means of a quantitative insight of the figures of merit of commercial laser-cut devices in order to provide the designers of future stent with the necessary tools and specifications to improve the performance and reliability of these devices.

2. Figures of merit of SX stents

This section investigates some of the main figures of merit associated with SX NiTi stents, highlighting key mechanical characteristics and

performance indicators essential for evaluating their effectiveness in clinical settings [64]. Each property plays a crucial role in determining the functionality and durability of stents within the dynamic environment of the human body. Understanding these figures of merit is essential for both stent designers and healthcare professionals to ensure optimal patient outcomes and minimize complications associated with stent implantation. In the following section, these properties will be explored in detail. These figures of merit are intended to help the designer to fully exploit the potential of AM technology in designing the new generation of stent and, to this end, the list focuses on the mechanical behavior of the stents rather than the clinic aspects, which can be evaluated only with proper trials. The figures of merit identified here are a comparison tool for various stent designs. In this work we decided to adopt an approach based on general definitions, without having a reference stent as a benchmark, due to the great variability in the design of commercially available stents.

2.1. Foreshortening

Once the stent is expanded radially, it becomes shorter in the axial direction because of the Poisson's effect, as shown in Fig. 6. The term used to describe this phenomenon is called foreshortening and can be calculated through the Eq. (1) where L_0 represents the initial stent's length before deployment in the vessel, while L_D represents the final length of the stent after it has been inserted in the blood vessel.

A stent with an excessive axial reduction is very difficult to precisely position at the atherosclerotic plaque site. This difficulty can lead to incomplete coverage of the plaque, causing damage to the thin endothelial layer and reducing the treatment's efficacy [8,65].

The axial misalignment, that in the most severe cases could also lead to the migration of the stent inside the vessel, is related both to the deployment procedure and to the foreshortening and it must be considered as one of the potential clinical problems which undermines the stent efficacy in restoring the vessel patency [66].

To enhance the performance of the stent, and have better clinical outcomes, foreshortening should be minimized [7,8], with the ideal target being zero.

$$Foreshortening = \frac{L_0 - L_D}{L_0} \tag{1}$$

2.2. Radial elastic recoiling

After releasing the stent from the catheter, it fully expands until it touches the vessel wall. Therefore, the pressure exerted by the vessel wall opposes the expansion of the stent, resulting in a reduction of the stent's diameter upon opening, as depicted in Fig. 7. The radial elastic recoil [67,68], quantifies this new equilibrium condition, which could also occur gradually after an extended period of time due to the viscoelastic behavior of the vessel. Radial elastic recoil is influenced by

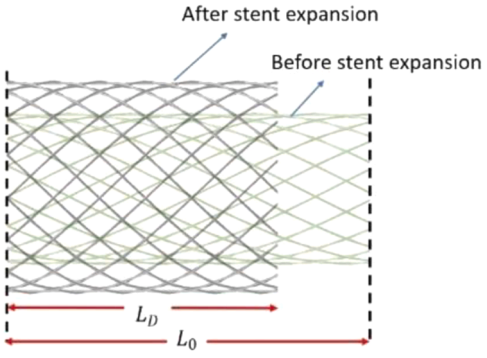

Fig. 6. Schematic of the foreshortening effect before and after the SX stent deployment, adapted from [30].

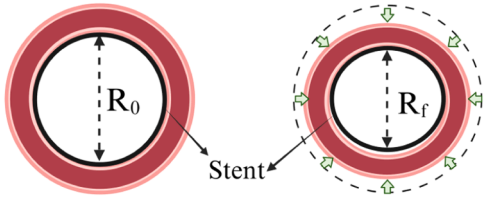

Fig. 7. Schematic representation of stent recoil, stent after deployment and full expansion (a) and stent after recoiling (b) due to vessel elastic springback.

different factors, including the design and material composition of the stent and its formula, in accordance to technical literature, is reported in Eq. (2), R_0 is the radial diameter of the stent when it reaches full expansion immediately after deployment, and R_f represents the final diameter of the stent in the last equilibrium position. The elastic recoil is strictly linked to radial stiffness. After deployment, if the stent shows high elastic recoil, it may lack the ability to adequately support blood vessels and maintain patency. Target value tends to zero or lowest possible.

$$R_{recoil} = \frac{R_0 - R_f}{R_0} \tag{2}$$

2.3. Dogboning

During vascular expansion, the stent undergoes non-uniform expansion which could cause vascular wall problems. This uneven deformation typically leads to the two ends of the stent being more open than the center, giving it a shape resembling a "dog bone" as shown in Fig. 8. This phenomenon happens since the proximal and the distal parts of the stent are less stiff than the central part of it. This occurs since the central part of the stent is supported from both sides, providing stability and rigidity, however, the two ends of the stent are only attached from one side, making them less supported and more prone to widening. Dogboning (D_b) can be calculated through Eq. (3) where D_{distal} is the maximum diameter of the stent at both distal or proximal part of it, while $D_{central}$ corresponds to the minimum diameter at the middle of the stent [69]. Uneven deformation at the distal ends results in substantial plastic deformation in those areas, leading to potential stent fracture and causing damage to the vessel at the stent edges, which in turn, contributes to restenosis [65]. Minimizing dogboning is essential to ensure uniform expansion across the entire stent. Target value is zero or negative.

$$D_b = \frac{D_{distal} - D_{central}}{D_{distal}} \tag{3}$$

2.4. Stiffness

Stents are designed specifically with the aim of upholding the patency of lumens (blood vessels, bile ducts, urethra) and they

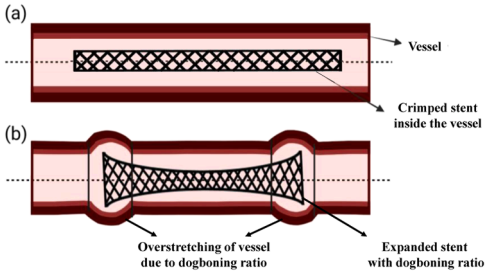

Fig. 8. Stent dog-boning mechanics schematic, adapted from [70]. (a) Crimped stent inside the vessel, and (b) expansion of the stent with an out of scale, which causes the artery to overstretch.

experience a combination of mechanical actions that twist, compress, elongate and bend them [71]. Femoro-popliteal district stents are mechanically the most stressed class of stents because femoro-popliteal district arteries (FPAs) twist and bend with almost any activity undertaken by the patient, including basic functions such as walking and sitting [72]. Due to the complexity and variety in design geometries of stents, SX NiTi stents of the same diameter and length can show very different stiffnesses, as evidenced by a number of studies which performed *in-vitro* (benchtop) tests to obtain the stiffnesses of various stent designs [48,72,73].

Fig. 9 depicts the main forces and moments acting on the stent after its deployment in the blood vessel, namely the axial force N, the bending moment M, the torque T and the radial pressure Δp. Therefore, four different stiffnesses (and consequently four compliances) can be envisioned: axial, bending, torsional and radial stiffness.

2.4.1. Axial stiffness

Axial stiffness, k_N and its inverse, axial compliance, c_N, is defined according to Eq. (4) where N is the axial force acting on the stent, Δl is the elongation (when positive) or shortening (when negative) of the stent in the axial direction, E is the Young modulus of the material (NiTi in the austenitic phase in this case), A is the equivalent cross-section of the stent and l is the length of the stent after its deployment in the blood vessel [74]. The experimental test rig is reported in Fig. 10 with tensile (Fig. 10a) and compressive (Fig. 10b) loading position.

$$k_N = \frac{N}{\Delta l} = \frac{EA}{l} = \frac{1}{c_N} \tag{4}$$

2.4.2. Bending stiffness

To assess stent bending stiffness, a common method used is the three-point bending test [75], in which the stent is bent under controlled conditions to evaluate its ability to flex without permanent deformation, usually under a three-point bending condition as showed in Fig. 10c-d. Bending stiffness, k_M, and its inverse, bending compliance, c_M, is defined according to Eq. (5) where M is the bending moment acting on the stent, φ is the bending angle of the stent, E is the Young modulus of the material (NiTi in the austenitic phase for this case), J_n is the second moment of the cross-sectional area of the stent around the x-axis, l is the length of the stent after its deployment in the blood vessel [74,76].

$$k_M = \frac{M}{\varphi} = \frac{EJ_n}{l} = \frac{1}{c_M} \tag{5}$$

2.4.3. Torsional stiffness

Torsional stiffness is an important factor mostly for stents designed for FPA stenoses [3]. Torsional *in-vitro* tests can be performed restricting axial deformations and executing tests with different angles or angular displacement rotations in both clockwise and counterclockwise directions with a chosen speed [48], as shown in Fig. 10e-f. Bending stiffness, k_T and its inverse, torsional compliance, c_T are defined according to Eq. (6) where T is the torque acting on the stent along the z-axis (namely the stent axis, which we assume is the same as the vessel axis), θ is the torsion angle, G is the shear modulus of the material (NiTi in the austenitic phase), J_O is polar moment of inertia of the stent, l is the length of the stent after its deployment in the blood vessel [74].

$$k_T = \frac{T}{\theta} = \frac{GJ_O}{l} = \frac{1}{c_T} \tag{6}$$

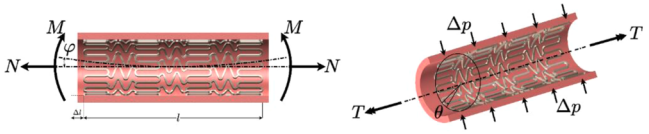

Fig. 9. Forces and moments acting on the stent.

2.4.4. Radial stiffness

Radial stiffness defines how the stent responds to changes in diameter with respect to external pressures. It is a measure of the ability of the stent to provide radial structural support against recoil within a blood vessel [26] and it is quantified by the variation of pressure over the diametral hoop strain as expressed in Eq. (7). In accordance with [77–79], Δp is the pressure the vessel exerts on the stent, ε_{hoop} is the hoop strain, d is the initial diameter of the stent, Δd is the diameter variation of the stent and c_r is the radial compliance of the stent [80].

$$k_r = \frac{\Delta p}{\varepsilon_{hoop}} = \frac{\Delta p \cdot d}{\Delta d} = \frac{1}{c_r} \tag{7}$$

Usually, radial stiffnesses are calculated as slopes of linear regression fits of loading curves obtained through experimental data [48]. The radial pressure and radial stiffness are strongly interdependent since this relationship relies not only on the absolute value of the pressure but also on the slope of the pressure-hoop strain curve. To demonstrate this, in Fig. 11, a comparison between two distinct stent designs is illustrated; curve A and curve B represent the mechanical behaviors of these designs under different radial pressures but the same diametral hoop strains. Curve B exhibits higher radial pressure but a slight slope, while curve A has lower maximum pressure at a given strain with a steeper slope. Despite curve A's lower maximum pressure, its steeper slope signifies a greater increase in pressure per change in diameter, suggesting higher radial stiffness than curve B ($k_{r,\ A} > k_{r,\ B}$). This comparison highlights that while the value of radial pressure often aligns with radial stiffness, the slope of the pressure-diametral hoop strain relationship profoundly influences the stent's overall mechanical behavior and greater maximum radial pressure does not necessarily translate to greater radial stiffness in stents. This behavior depends both on geometry and on the material model, which follows a superelastic curve.

While high radial stiffness is essential to prevent arterial collapse by enhancing the ability of the stent to restore blood flow and prevent it from recoiling [48,81], low radial stiffness is important for minimizing stress on vessel walls and reducing the risk of inflammation and restenosis. Therefore, achieving an optimal trade-off between high and low values of radial stiffness is key in stent design to ensure both structural support and vessel wall health.

2.5. Oversizing

A SX stent is often chosen with a diameter slightly larger than the vessel's diameter to serve its function effectively within a blood vessel and prevent migration [82]. The ratio between the initial stent diameter (D_s) and the vessel inner diameter (D_v) is called oversizing (OS), which can be calculated from Eq. (8). Clinical observations and studies suggest that for SX NiTi stents, oversizing ratios in the range of 1.1–1.4 lead to improved lumen gain, reduced incomplete stent apposition, and favorable long-term fatigue performance [82–85]. On the other hand, an increase in the oversizing ratio beyond this ideal range ($OS > 1.4$) can result in high radial forces, potentially causing damage to the artery wall and compromising the stent's long-term efficacy including collapse.

$$OS = \frac{D_s}{D_v} \tag{8}$$

2.6. Radial forces

Radial forces, whether exerted on the stent or by the stent onto the vessel wall, are critical to the design and function of stents, making it essential to understand their significance for optimizing stent design and deployment strategies. In the following section, the significance of three main radial forces listed below and illustrated in Fig. 12a-c, is described:

- Radial Resistive Force (RRF)

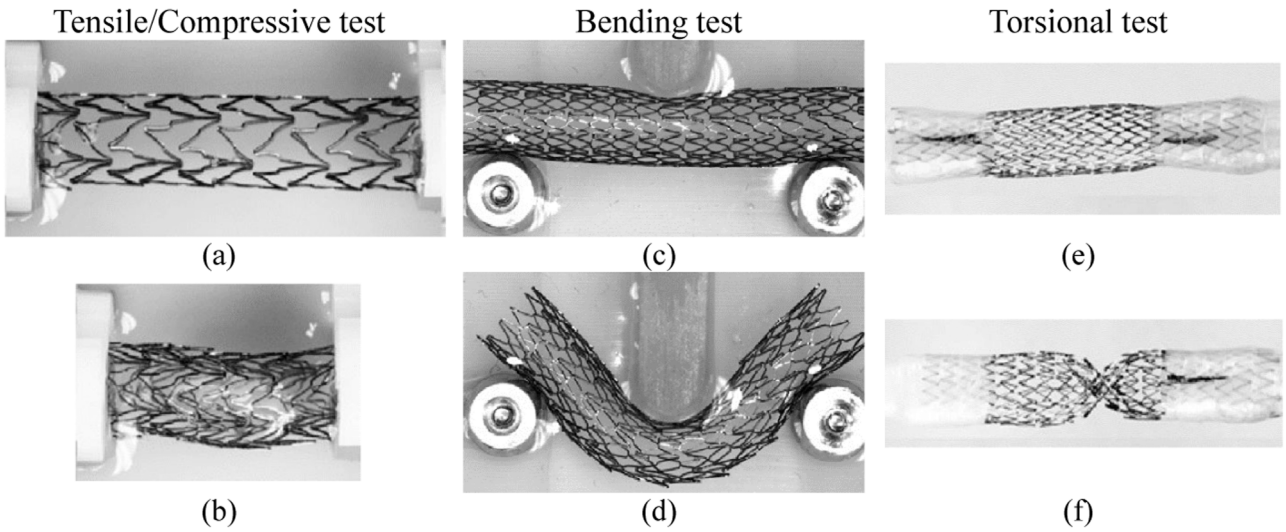

Fig. 10. Stent testing according to [48]. Axial test: (a) tensile load and (b) compressive load. Bending test: (c) neutral position and (d) load pin displacement applied to the middle of the span. Torsional test: (e) neutral position and (f) 90°/cm torsion.

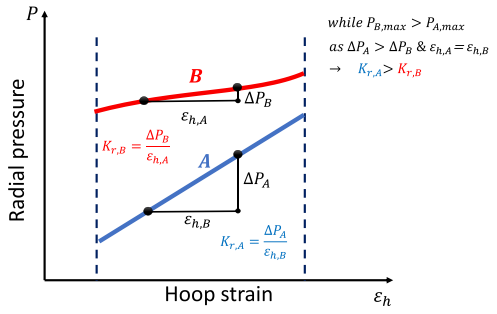

Fig. 11. Comparison of radial pressure-hoop strain, curve A with low pressure and high stiffness and curve B with low stiffness and high pressure.

- Chronic Outward Force (COF)
- Crush Resistance (CR)

2.6.1. RRF

As already mentioned, when a SX stent is designed, it's often manufactured in a larger size than vessel diameter to serve its function effectively within a blood vessel (point 1 in Fig. 12d). However, to deliver it to the target location within the vessel, it needs to be crimped to a smaller size to fit into a delivery catheter (point 2 in Fig. 12d). The force required to achieve this compression is called the radial resistive force (RRF). RRF describes the force that is required to compress the stent radially during circumferential loading (crimping) to fit the catheter. To maintain the stent diameter and reduce the risk of restenosis, a stent must have enough RRF [86,87]. However, the precise amount of RRF needed *in-vivo*, is still debated [48] since it depends on the stent-wall interaction.

2.6.2. COF

When the stent is removed from the catheter and inserted into the vessel, it expands, as shown by Fig. 12d from point 2 until the expansion is stopped by the contact to the vessel wall (point 3 in Fig. 12d). At this point the stent and the vessel reach a stress equilibrium, and the stent cannot expand anymore. Therefore, it continues to exert a continuous outward force onto the vessel wall known as chronic outward force (COF). The COF is the force that the stent exerts on the vessel wall when it undergoes expansion (during unloading) [86]. Although low COF on the vessel ensure vessel patency and prevents stent migration and restenosis [88], excessive COF has the potential to cause avoidable

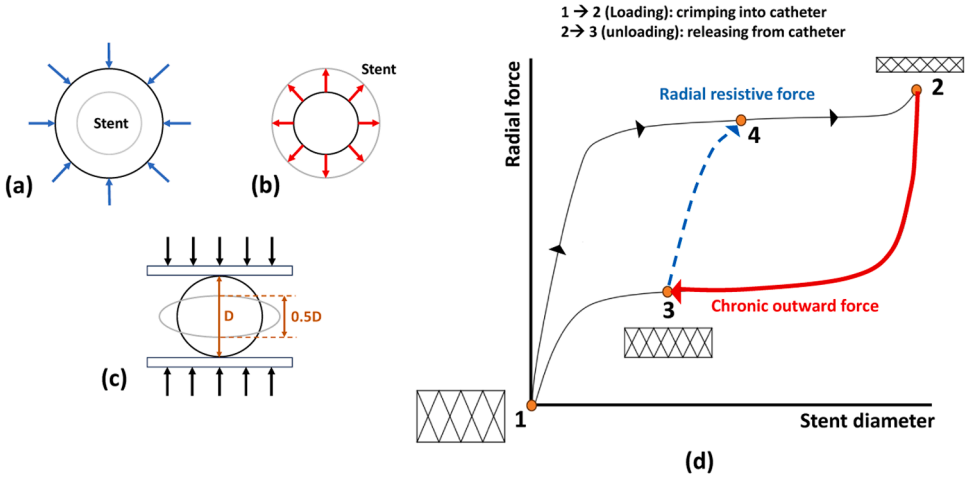

Fig. 12. (a) Schematic illustration, adapted from [38], of the compression mechanism during the testing of (a) radial resistive force, (b) chronic outward force, (c) crush resistance force, and (d) radial resistive and chronic outward force as a function of the superelastic hysteresis loop, adapted from [90].

damage to the surrounding tissue [48,64].

Elastic hysteresis of NiTi allows for a continuous COF on the vessel wall which remains very low even when subjected to significant deformations. In contrast, the stent's ability to resist compression, which is represented by RRF, increases rapidly as the stent deforms until it reaches a plateau stress level (as shown in Fig. 12d, from point 3 to point 4). This dynamic interplay between COF and RRF showcases Nitinol's capability to provide effective support while minimizing the risk of vessel damage, making it a valuable material for stent design and deployment. Generally, stent designers attempt for the maximum achievable RRF while keeping the COF to a minimum [28]. Both characteristics of RRF and COF were analyzed using the radial force-tester method [75].

2.6.3. CR

The last parameter has a simpler definition: crush resistance (CR) is the force required to compress the stent in one radial direction [88] as shown in Fig. 12c. To measure CR, the stent is compressed between parallel plates from its expanded state up to a 50% diameter reduction [89]. The main issue related to CR is that insufficient CR raises the risk of restenosis [87].

The experimental setup required to estimate the radial force is not trivial. A couple of examples are reported in Fig. 13, where a special machine is exploited Fig. 13a or a test rig with rollers and a thin aluminum sheet is used to apply a *quasi*-uniform compressive pressure on the stent Fig. 13b.

2.7. Fatigue life of stents

Once implanted, stents are subjected to continuous loadings due to pulsatile cardiac pressure within the bloodstream. Furthermore, depending on the region in which they are implanted, they can be subjected to bending, compression, and torsion. For example, several *in-vivo* tests on cadavers showed that during hip flexion and knee bending, the superficial femoral artery (SFA) and the popliteal arteries are subjected to axial compression and bending [91,92]. Most of the bending occurs behind the knee, but some bending also occurs on the straight tract of the SFA. Over time, the continuous pulsatile and mechanical stresses can induce fractures in stents. In regions such as the FPA bending occurs in the order of magnitude of 10^6 cycles per year [24]. According to 1995 FDA guidelines [20,26] when implanted in SFAs, stents would need to be certified for at least 400 million cycles without a single fracture. Fatigue of stents, being a very complex subject, is still an open problem for NiTi, although several works exist on assessing the fatigue behavior of stents [20,24,93] through finite element analysis (FEA) in order to predict their *in-vivo* fatigue resistance.

Although changing the design of the stent can affect its fatigue life, most studies are devoted to improving the fatigue life of the base material [20]. For metals such as steel or linear elastic materials in general, a stress-based approach [10] such as Wohler curves is used, but for NiTi and superelastic materials in general, a strain-based approach is preferred in order to consider the superelastic behavior of the material.

Therefore, a possible factor of safety (FOS) definition for a NiTi stent is shown in Eq. (9), where ε is the critical strain amplitude of the material and ε_a is the strain amplitude withstood by the stent during its life. [20,94]. The critical strain amplitude experimentally measured for NiTi is around 0.4–0.55 % [20,95] for mean strains below 3 %, which is a compatible range for stent devices. Fatigue is also strongly dependent on the surface finish of stents which explains the very precise and careful polishing and etching of the stent which reduces the roughness of metal and improves the fatigue performance.

$$FOS = \frac{\varepsilon}{\varepsilon_a} \tag{9}$$

2.8. Wall shear stress

This last figure of merit is the only one related to the hemodynamic and not to the mechanical properties of the device, which is very important since it affects the stent performance. Generally, a vessel wall is subjected to two main forces. First, the blood within the vessel exerts pressure outward onto the wall of the vessel known as blood pressure, leading to circumferential stress. Secondly, as blood flows through the vessel, it creates a frictional force along the inner surface of the vessel. This frictional force, generated by the blood flowing in the vessel wall in tangential direction, is called wall shear stress (WSS) [96,97]. The shear stress levels vary within different segments of the circulatory system. In the venous system, shear stress typically ranges from 0.1 to 0.6 Pa, whereas in the arterial vascular network, it generally varies from 1 to 7 Pa [98]. In context of stent implantation, the insertion of the stent in a blood vessel can lead to additional stress on the vessel wall [97]. This additional stress leads to changes in the normal blood flow and local shear distribution which in turn causes implications for the overall hemodynamic performance of the vessel and may influence factors such as neointimal proliferation and restenosis.

When a stent is deployed, it alters the natural geometry of the artery, leading to changes in blood flow patterns. Specifically, the increased curvature at the stent's edges can result in regions where blood flow becomes turbulent or oscillatory [99]. Furthermore, the increase in diameter of the stent after deployment may reduce blood velocity, potentially exacerbating adverse hemodynamic conditions that contribute to restenosis [100]. Research has shown that the design parameters of the stent, particularly the number and dimensions of struts, surface topology and the stent-to-artery deployment diameter significantly influence WSS and clinical outcomes such as neointimal

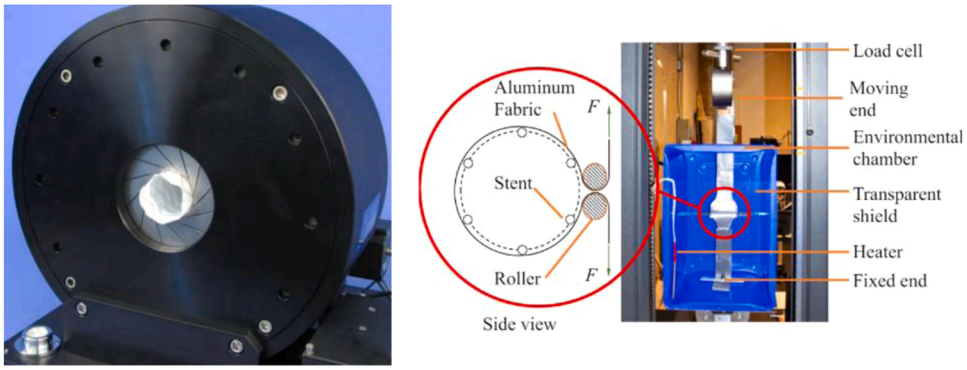

(a) (b)

Fig. 13. Radial force measurement of a stent: (a) radial RX-650 with several blades to radially compress the stent uniformly [88], (b) a stent wrapped in a sheet in a circular configuration attached to tensile machine grippers radially compressing the stent [77].

hyperplasias and restenosis [101–103]. For instance, a higher stent-to-artery deployment ratio can increase exposure to WSS compared to a lower ratio [101]. Moreover, increasing the height and number of struts can generate disturbed WSS zones, while reducing strut thickness can decrease areas subjected to WSS [101]. Thinner struts generally lead to improved re-endothelialization. Research indicates that thicker struts create more disturbed flow patterns and higher shear stress levels, which can delay endothelial healing and increase the risk of thrombosis and restenosis [104,105]. For instance, a study [99] highlighted that thicker bioresorbable stents resulted in delayed re-endothelialization compared to thinner drug-eluting stents.

Hemodynamic performance of stents is often evaluated by a WSS index, quantifying the impact of in-stent restenosis [67,106]. This index is calculated through Eq. 10, where n is the normal vector to the vessel surface and $\overrightarrow{\overrightarrow{\tau_{ij}}}$ is the fluid viscous stress tensor [107]. An ideal stent design should aim to achieve superior biological hemodynamic performance with minimal changes to laminar blood flow properties and WSS distributions.

$$\tau_w = n \bullet \overrightarrow{\overrightarrow{\tau_{ij}}} \tag{10}$$

2.9. General discussion on the figures of merit

The effectiveness of SX NiTi stents is dependent on several key mechanical properties and performance metrics, as discussed in this section. These figures of merit are crucial for evaluating stent functionality and durability within the vessels. To facilitate stent design and optimization, it is essential to establish desired optimal values (or ranges) for each of these properties to serve as benchmarks for stent designers and manufacturers, guiding them towards achieving optimal performance while minimizing potential complications associated with stent implantation. Table 1 provides a summary of the desired values of each parameter, offering valuable insights for enhancing the efficacy and reliability of SX NiTi stents in clinical settings. Based on Table 1, an ideal stent should exhibit zero foreshortening, dogboning, and elastic recoil, although achieving this is challenging, particularly concerning dogboning and recoiling parameters. Yet, advancements in stent design offer promising strategies to mitigate these issues. In minimizing foreshortening, research has shown promising results, for instance P.K.M. Prithipaul et al. achieved zero foreshortening with some hybrid auxetic cell design in their study [67]. Addressing dogboning, a balance in the radial stiffness of the middle and end parts of the stents should be adjusted, which can be done either by increasing the thickness of the struts on the ends of the stents [108,109] or by adding closed-cell segments to those parts of the stent to make them stiffer. To prevent recoiling, the higher the radial stiffness of the stent, the more resistant it can be to the pressures from the vessel wall and the less recoiling. Therefore, increasing the radial stiffness can effectively prevent stent recoil. On the other hand, excessive radial stiffness can reduce stent compliance and apply high radial pressure to the vessel wall, resulting in damage to the vessel and therefore causing ISR. Therefore, based on the amount of pressure and the radial force that the vessel can withstand, which strongly depends on the vessel positions, it is possible to increase the stiffness of the stent to a certain extent. Similarly, the RRF range should be carefully selected to push away the plaques and keep the vessel open effectively without causing vessel damage. Oversizing can have a significant effect on the amount of RRF. Higher oversizing leads to higher RRF. Typical endovascular procedures suggest to apply the slightly larger stent available, but applying a 10 mm stent on a 9 mm vessel causes an RRF and a COF lower than 10% compared applying a 6 mm stent on a 5 mm vessel, according to Eq. (8). Since commercial stents are commonly shelf devices with predefined dimensions it is hard to prescribe an optimal solution. In addition, an ideal stent should maintain normal blood flow. In other words, it should not increase further WSS on the vessel wall. Despite the inevitable changes in WSS caused by stent implantation, the design of the stent can be optimized to reduce its impact on WSS. By designing the stent with smooth edges and ensuring that struts are aligned as parallel as possible to the vessel direction, the likelihood of disturbing blood flow and increasing WSS is reduced [103]. In conclusion, optimizing the mechanical properties and performance metrics outlined in Table 1 is essential for enhancing the efficacy and reliability of SX NiTi stents.

To summarize, thirteen figures of merit for describing SX NiTi endovascular stents were analysed, qualitatively and, where possible, quantitatively. Specific quantitative ranges for each figure of merit were not provided, given the wide variety of regions in which endovascular stents can be deployed. Each of these district requires the optimization of some specific characteristics of the stent (for example, a stent for the FPA requires greater bending compliance than a stent for the SFA). Only oversizing is given a more precise range of values, since a general trend of applicability was found in the stent applications guidelines [85].

Table 1
Desired values for SX NiTi stents.

Figures of merit (unit)	Desired value	References
Foreshortening (%)	Minimum the best	[7,8]
Radial elastic recoil (%)	Minimum the best	[67]
Dogboning (%)	Minimum the best	[65]
Radial stiffness (MPa)	Nominal the best	[48,81]
Axial stiffness (N/mm)	Minimum the best	[48]
Bending stiffness ($N \bullet mm/rad$)	Minimum the best	[8,48]
Torsional stiffness ($N \bullet mm/rad$)	Minimum the best	[48]
Oversizing (%)	$10\% < OS < 40\%$	[82–85]
Radial resistive force (N)	Nominal the best	[48]
Chronic outward force (N)	Minimum the best	[28,48]
Crush resistance (N)	Maximum the best	[87]
Fatigue life (number of cycles)	Maximum the best	[20,78,110]
Wall shear stress (Pa)	Minimum the best	[97,100,111]

3. Classification of stents based on geometry

From the point of view of the shape, stents are grouped into coil, slotted tube, and modular designs [112]. Coil stents are constructed using wires that are shaped and arranged into a circular coil configuration to form the stent scaffold. In the case of slotted tube stents, a metal tube acts as the stent's basis material, and a specific design or pattern is generated using laser cutting [30,32]. The modular stent's construction involves interconnected individual modules, allowing for a more customizable and adaptable structure. This last design is intended to overcome specific challenges present in traditional stent designs. For instance, it addresses the poor radial force and higher restenosis rates associated with coil stents, as well as the drawbacks of slotted tube stents, which may have low bending compliance and deliverability. The modular design provides a balance between the bending compliance of coils and the radial strength of slotted-tube designs [9]. In Fig. 14, a schematic classification of stents alongside images illustrating representative examples of each stent type are presented.

Modular ring stents are classified into three groups: closed-cell, open-cell, and hybrid-cell. Closed-cell designs (Fig. 15a) are characterized by interconnected stent strut with smaller free cell area, while the open-cell designs (shown in Fig. 15b) have larger free cell area with fewer interconnections [112,113]. Additionally, there are also hybrid-cell configurations that combine these first two groups to gain the benefits of both designs [114], mostly with the same design at proximal and distal segments and a central different cell design (Fig. 15c-d). Hybrid stents, such as Scitech Solaris, have an open-cell design in the central part, for improving the bending compliance of

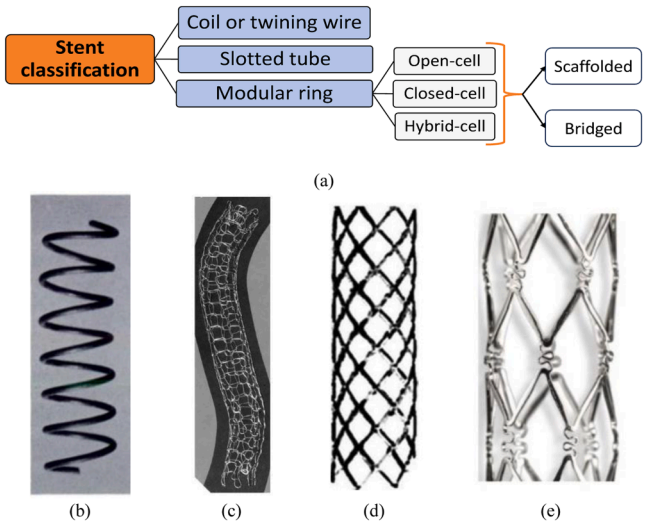

Fig. 14. (a) Schematic classification of stents based on the geometry, (b) Nitinol coil wire stent by Dotter et al. [5], (c) Strecker stent made of knitted tantalum wire [116], (d) slotted tube structure of Palmaz-Schatz stent [76], (e) a modular ring with closed-cell design [117].

the stent, and a closed-cell design at the two ends to adjust the stiffness in the distal parts (as depicted in Fig. 15c). Other hybrid stents such as Cristallo Ideale, a Medtronic carotid stent [115], combine open-cell design at the proximal and distal sections (as shown in Fig. 15d) enhancing conformability, flexibility and reducing radial force in the healthy vessel segments. The closed-cell design in the central part secures the appropriately high scaffolding at the lesion site preventing plaque prolapse.

More gaps between the cells in an open-cell design makes it more compliant compared to a closed-cell design, which is particularly advantageous for complex arteries with angular or twisted anatomies [116]. On the other hand, as the closed-cell design has more interconnections, it is stiffer, offering better plaque coverage and structural support [114,118]. However, this increased stiffness comes with potential drawbacks such as higher risk of restenosis post-stenting. Another difference regarding hemodynamics properties is that a closed-cell stent allows for a higher blood flow velocity through the stented region compared to an open-cell stent structure [119]. A summary of the differences between open-cell and closed-cell stent designs is provided in Table 2.

The last geometrical considerations regard the scaffolded or bridged structures. The former are characterized by the direct connection and arrangement of representative unit cells (RUC) as in Fig. 16a. On the other hand, bridged structures, as depicted in Fig. 16b are composed of bridge/connector and rings. In this design, rings play a pivotal role in radially expanding and providing support to the blood vessel, while bridges/connectors connect the rings axially, contributing to the stent's axial stiffness [123]. Each ring is typically composed of circumferential struts as shown in Fig. 16c.

Understanding the impact of strut and bridge topology on stent performance is one of the crucial factors for stent design. Researchers commonly concentrate on optimizing stent performance by investigating factors such as the shape, arrangement, and number of bridges, along with the width, thickness, and length of the struts, so providing insight on this factor is helpful, hence the compact form shown in Table 3. Generally, a decrease in the number of bridges/connectors between struts tends to enhance the bending compliance of the stent [124]. Moreover, according to some clinical studies, stents with the higher thickness of the strut are associated with the higher risk of restenosis in the vessel [125–127]. Additionally, aligning the struts parallel to the blood flow helps in maintaining a more uniform distribution of WSS within the vessel [103]. While different strut dimensions may imply different impacts on the stent's performance such as stiffness, radial forces, etc., they do not affect the foreshortening, as the foreshortening is dependent on the cell geometry and affected by the angle between the stent's strut and the axial direction of the stent [128].

4. Analysis of commercial self-expanding NiTi stents

This section provides an analysis of a selection of commercial SX NiTi stents, based on their geometry and the previously described figures of merit. These stents may be found for both arterial and venous applications. However, the stent design must carefully consider the unique characteristics of veins and arteries. While both are integral components of the circulatory system, they exhibit distinct differences in function, structure, mechanical properties, flow patterns, and pathologies [77, 133,134]. Therefore, to ensure optimal performance and efficacy, stent designs must be tailored to accommodate these features, reflecting the specific demands of each vascular environment. Therefore, the comparison provided is separated for arterial or venous applications.

4.1. Arterial stents

Research on arterial stents is more extensive than on venous ones due to the fact that they are more commonly used. The majority of studies on coronary stents, carotid stents, SFA and FPA are devoted to *in-vitro* [10, 72] or numerical tests trying to reproduce the behavior of an existing stent [24]. Since this work is aimed primarily at examining the engineering aspects related to stent design, prominence was given mostly to the latter studies rather than to clinical tests which are devoted to purely medical considerations. Table 4 compares the geometric characteristics of nine different commercially available NiTi SX arterial stents. Cook Medical Zilver (518 or 635, depending on the size of the catheter, Fig. 17a), is used as an adjunct to PTA in the treatment of symptomatic vascular disease of the iliac arteries. Cordis S.M.A.R.T. CONTROL (Fig. 17b) is used to treat iliac, femoral, and proximal popliteal lesions. Biotronik Pulsar (18 or 35, depending on the size of the catheter, Fig. 17c) is recommended for use in patients with atherosclerotic disease of the femoral and infrapopliteal arteries. GORE TIGRIS (Fig. 17d), was intended to improve luminal diameter in patients with symptomatic de novo or restenotic lesions or occlusions in the SFA and the FPA. It is a discontinued product (it has been replaced by another SX stent called VIABAHN), but it was considered in this study due to the wealth of data provided on it in the literature. Boston Scientific Innova (Fig. 17e) is used for the treatment of SFA lesions. All stents compared in the following table are laser cut, except Abbott Supera (Fig. 17f), which is manufactured with interwoven wire technology. This peculiar stent is used in the case of SFA lesions and lesions of the FPA. Abbott also produces laser-cut stents, and Abbott Absolute Pro (Fig. 17g) is a laser-cut SX stent indicated for the treatment of iliac arteries. Two more stents included in this comparison used in the treatment of atherosclerotic lesions in the SFA and popliteal artery are Medtronic EverFlex and BD Lifestent (Fig. 17h-i).

The diameters and lengths of the stents compared are reported, together with their strut thickness (where possible) and the stent cell design (open, closed, or hybrid) architecture. It can be seen that diameters have a range of 4–14 mm, depending on the typical application zone of each stent; for example, Cordis S.M.A.R.T. has a range of diameters that go from 6 to 14 mm, and it is suitable to treat both the iliac arteries (mean diameter of 11.8 mm) and FPAs (mean diameter of 6.9 mm) [136].

More interesting to note is the strut thickness variability. A lower strut thickness is normally preferred, but the technological limitations are important. The average dimension is around 190 microns with a quite low variation (± 15 %). This data is particularly interesting for the designer since it provides a baseline for this application.

In Table 5 we summarized the results of different benchtop tests

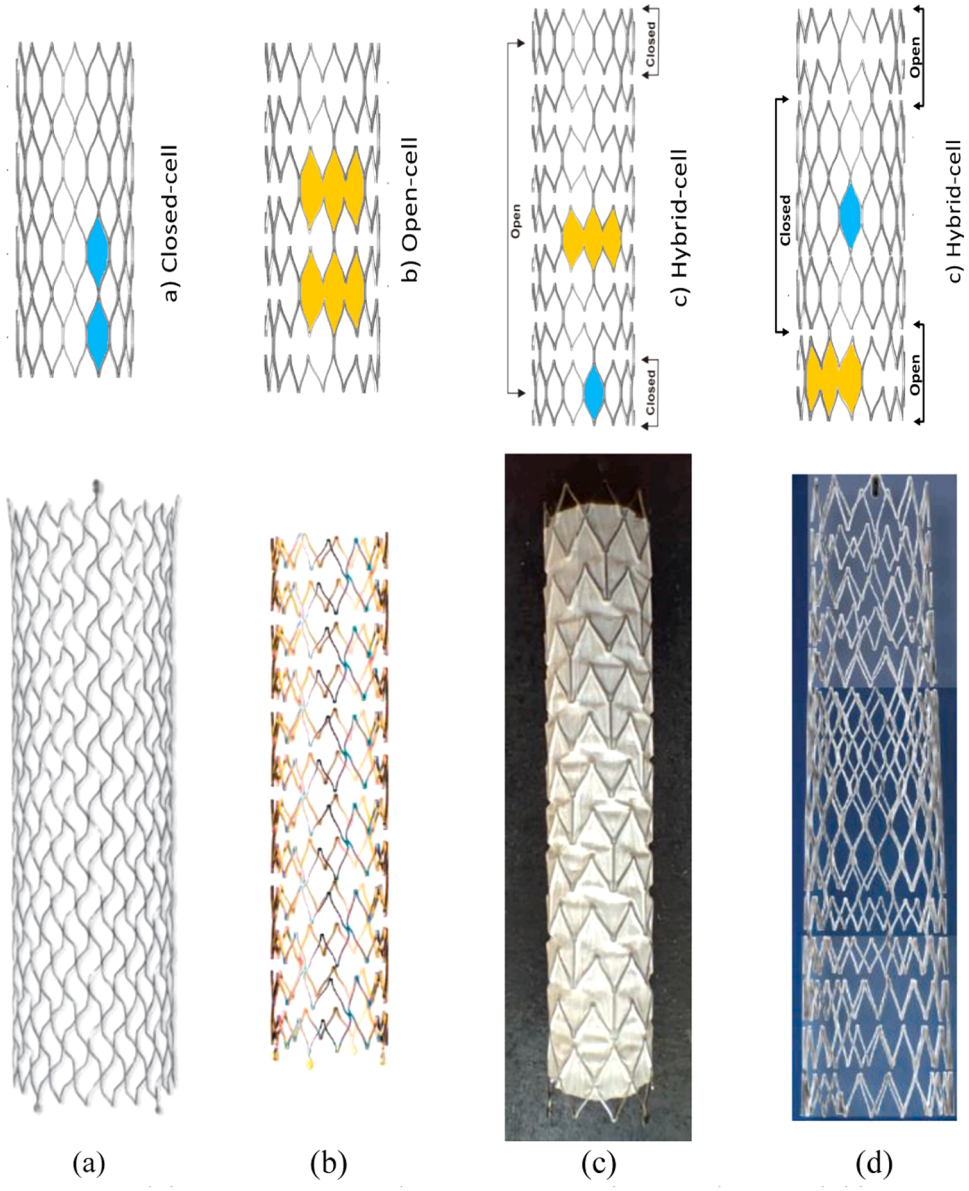

Fig. 15. Modular stent arrangements, adapted from [120], with corresponding available stents: (a) closed-cell, Optimed Sinus-XL [121], (b) open-cell, Biotronik Pulsar [115,122], and (c-d) hybrid-cell configurations, Scitech Solaris, Medtronic Cristallo Ideale [115].

Table 2
Comparison of parameters between open-cell and closed-cell stent designs.

	Open-cell stents	Closed-cell stents
Compliance	↑	↓
Radial stiffness	↓	↑
Applicability for complex vessel	↑	↓
Plaque coverage	↓	↑
Higher risk of restenosis	↓	↑
Velocity of blood flow after stenting	↓	↑

taken from various articles of literature that compared arterial stents. The references are reported in the table as well.

The average RRF is around 0.530 N/mm with a variation of ± 45 %. The average COF is around 0.381 N/mm with a variation of ± 38 %. The average CR, excluding the outlier Abbott Supera (which is a braided stent, resulting in a CR of an order of magnitude bigger than laser-cut stents), is around 0.074 N/mm with a variation of ± 25 %.

C. Brandt-Wunderlich et al. [89], tested and compared six SX NiTi stents in terms of CR and RRF, at 1 mm oversizing and at 2 mm oversizing. All stents had a diameter of 6 mm and a length of 80 mm. Their results highlighted that the compared stents having a high CR showed also a high RRF, and vice versa, with one exception (Abbott Absolute Pro). Stents that show high RRF and CR could be considered a marker of radially stiff stents, capable of keep the patency of the vessel, but they could cause vessel injuries due to vascular overdilatation; on the other hand stents with lower RRF and CR could reduce vascular irritations, but could have too low radial stiffnesses, which would not allow the correct patency of the vessel to be maintained [89]. This is consistent with what we discussed in the figures of merit section of this article. In addition, W. Schmidt et al. [72], compared 6.0x80 mm SX stents but for SFA instead of FPA. Their results showed that stents with small and closed cells resulted in higher radial support with respect to stents with large and open cells as well as a low number of V-shaped strut segments with long struts [72]. Among other metrics (such as trackability, pushability, and radiopacity), we decided to collect the thicknesses of the struts, the crush resistance at 50 % diameter reduction and the chronic outward force values with 1 mm oversize, normalized to the length of the stent,

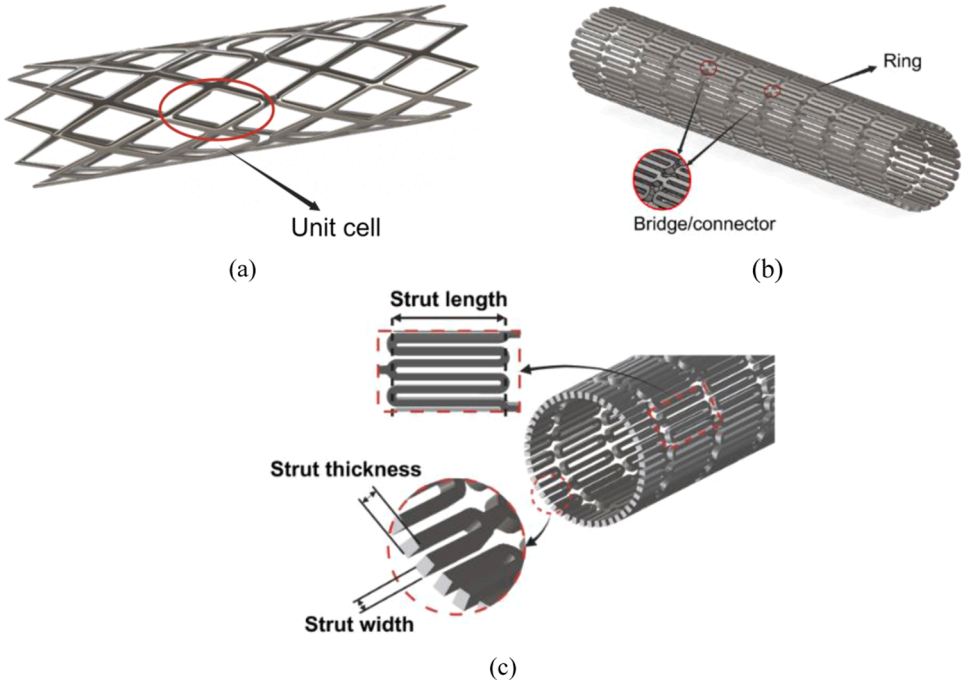

Fig. 16. Two types of modular stents: (a) scaffolded structure [129], (b) bridged structure [130]. (c) Cross-sectional view of a segment of the stent illustrating strut dimensions.

Table 3
The effects of strut dimensions on the figure of merits of stents.

	Strut dimensions			References	Note
	↑ Width	↑ Thickness	↑ Length		
Foreshortening	-	↓	-	[128]	Depends on the cell geometry: considering same displacement in radial direction
Recoiling	↓	↓	↑	[108]	Stiffer stents cause lower recoiling
Dogboning	↓	↓	-	[108,109]	Increasing width and thickness of the strut selectively at both stent ends reduces dogboning
Radial stiffness	↑	↑	↑	[131]	
Axial, torsional, and bending stiffness	↑	↑	↓	[124,132]	
Oversizing	-	-	-	[82]	Depends on the stent/vessel diameter
RRF, COF, CR	↑	↑	↓	[68,132]	
Fatigue life (isostress)	↑	↑	↓	[131]	Mechanical tests at same load
Fatigue life (isostrain)	↓	↓	↑	[132]	Mechanical tests at same displacement
Wall shear stress	↑	↑	-	[101]	Larger struts cause more flow turbulence

Table 4
Comparison of commercial SX arterial NiTi Stents: a geometric analysis.

Model (Brand)	Use	Cell design	d (mm)	l (mm)	t (μm)	Ref.
Zilver (Cook Medical)	Symptomatic vascular disease of the iliac arteries	Open-cell	6–10	20–80	192	[122]
S.M.A.R.T. CONTROL (Cordis)	Iliac and femoro-popliteal lesions	Open-cell (micromesh design with a multi segmental construction)	6–14	20–150	197.11	[72]
Pulsar (Biotronik)	Atherosclerotic disease of the femoral and infrapopliteal arteries	Open-cell (peak-to-valley design and S-articulating connecting bars)	4–7	20–200	153.07 140	[72, 122]
TIGRIS[1] (GORE)	Treatment of SFA and FPA	Open-cell with external fluoropolymer lattice	5–8	30–100	N.A.	[135]
Innova (Boston Scientific)	Treatment of SFA lesions	Hybrid-cell architecture (closed-cell ends open-cell center)	5–8	20–200	223.45 213	[72, 122]
Supera (Abbott)	SFA and FPA lesions	Interwoven wire technology	4.5–7.5	20–200	182.33 178	[72, 122]
Absolute Pro (Abbott)	Iliac arteries	Hybrid-cell design (closed-cell end segments)	6–10	20–200	181.75	[72]
EverFlex (Medtronic)	Peripheral arterial disease in the SFA and FPA	Open-cell, spiral cell connection pattern	6–8	20–150	228	[122]
LifeStent (BD)	Atherosclerotic lesions in the SFA and FPA	Open-cell, helical design	5–7	20–170	192	[122]

[1]Discontinued, replaced by VIABAHN

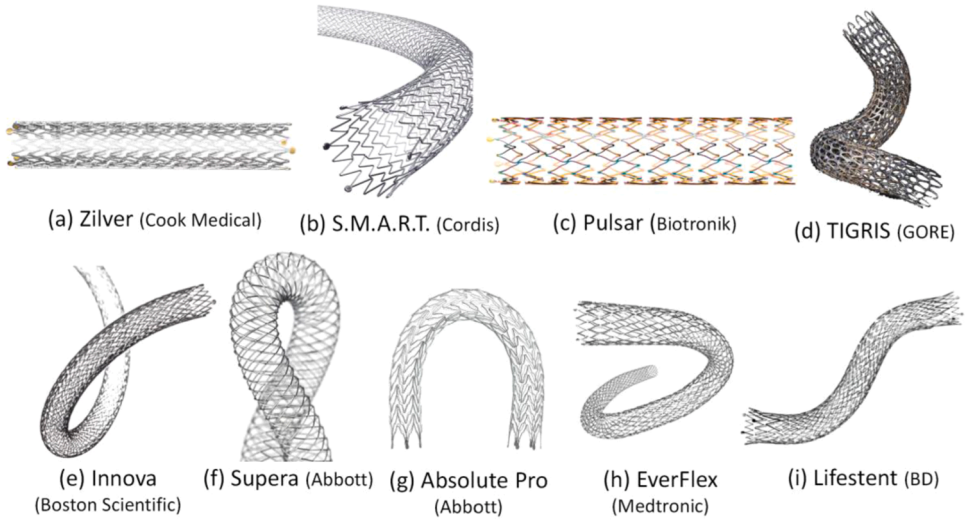

Fig. 17. Commercial SX NiTi arterial stents: (a) Cook Medical Zilver [137], (b) Cordis S.M.A.R.T. [138], (c) Biotronik Pulsar [122], (d) GORE TIGRIS [135], (e) Boston Scientific Innova [139], (f) Abbott Supera [140], (g) Abbott Absolute Pro [141], (h) Medtronic EverFlex [142], (i) BD Lifestent [143].

Table 5
Comparison of commercial SX arterial NiTi stents: mechanical properties.

SX arterial stents	Open-cell						Closed-cell	Hybrid-cell	Braided	Ref.
	Zilver	S.M.A.R.T. CONTROL	Pulsar	TIGRIS	LifeStent	EverFlex	Innova	Absolute Pro	Supera	
RRF (N/mm)	N.A.	0.773	0.242	0.610	N.A.	N.A.	0.777	0.250	N.A.	[89]
COF at 1 mm oversizing, normalized to stent length (N/mm)	0.29	0.389	0.133, 0.25	0.406	0.57	0.56	0.5030.49	0.214	N.A.	[72, 122]
CR at 50 % diameter reduction (N/mm)	N.A.	0.078	0.038	0.088	N.A.	N.A.	0.087	0.080	0.73	[72]
Force needed to stretch 50 % lengthwise (N)	1.34	2.99	N.A.	N.A.	0.80	1.76	1.25	0.68	N.A.	[144]

where the producers disclosed the information.

4.2. Venous stents

Research into ideal venous stents is still a relatively new area when compared to arterial stents, yet some studies have been conducted [77, 133,145]. In Fig. 18, the pictures of some commercial venous stents are depicted, namely: Bard E-Luminexx (Fig. 18a), Cook Zilver Vena (Fig. 18b), Optimed Sinus Venous (Fig. 18c), Sinus Obliquus (Fig. 18d), Sinus XL (Fig. 18e), Sinus XL Flex (Fig. 18f), Veniti Vici (Fig. 18g), Bard Venovo (Fig. 18h), Medtronic Abre (Fig. 18i). In addition, the dimensional information and technical details of the aforementioned stents are given in Table 6. Although the focus of this study is on NiTi stents, we also decided to consider Wallstent (Boston Scientific, USA) even though

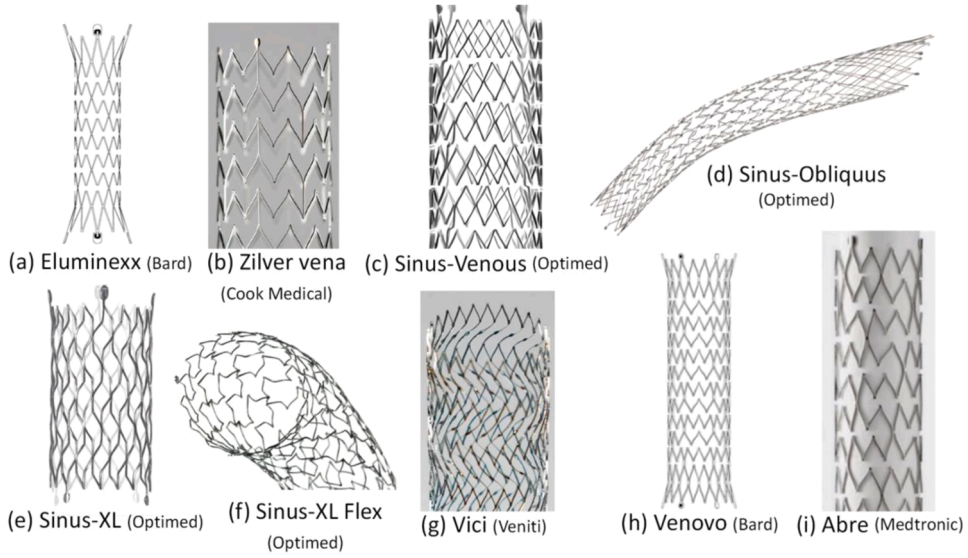

Fig. 18. Commercial SX NiTi venous stents: (a) Bard E-Luminexx [149], (b) Cook Medical Zilver Vena [164], (c) Optimed Sinus-Venous [165], (d) Optimed Sinus-Obliquus [152], (e) Optimed Sinus-XL [121], (f) Optimed Sinus-XL Flex [156], (g) Veniti Vici [166], (h) Bard Venovo [146], (i) Medtronic Abre [162].

Table 6
Comparison of commercial SX venous stents: a geometric analysis.

Model (Brand)	Intended use	Cell design	d (mm)	l(mm)	t(μm)	Ref.
Wallstent (Boston Scientific)	Off-label design, used for both arteries and veins	Braided, wire-based stent	5–24	23–145	330	[77,148]
E-Luminexx (Bard)[2]	Iliac occlusive disease in patients with symptomatic vascular disease of the common and/or external iliac arteries	Diamond cell, open-cell design with 2 mm flared stent ends	7–10	20–100	220	[77,149]
Zilver Vena (Cook Medical)	Obstructed iliofemoral veins	Chevron, open-cell design	10–16	40–140	220	[77,150]
Sinus Venous (Optimed)	Iliofemoral veins, post thrombotic syndrome, deep vein thrombosis, tumor related stenosis	Open-cell design	10–18	60–150	335	[151]
Sinus Obliquus (Optimed)	Symptomatic obstructions of the iliac veins, obstructions close to bifurcation of inferior vena cava	Hybrid-cell: closed-cell design at distal and proximal segments, open-cell design in the middle. Oblique distal part	14–18	80–150	335	[152,153]
Sinus XL (Optimed)	Aortic stenosis and dissections, vena cava compression syndrome, obstructions of the vena cava	Closed-cell design, ideal for straight sections	16–36	30–100	N.A.	[121, 153–155]
Sinus XL Flex (Optimed)	Obstructions of the curved segments of the inferior and superior vena cava, iliac vein, femoral vein, abdominal aorta	Open-cell design, ideal for curved sections	14–24	40–150	N.A.	[156,157]
Vici (Veniti)[3]	Iliofemoral venous obstructive disease	Closed-cell design	12–16	60–120	N.A.	[158]
Venovo (Bard)	Symptomatic iliofemoral venousoutflow obstruction	Open-cell design with 3 mm flared stent ends to reduce migration risk	10–20	40–160	N.A.	[146,153, 159,160]
Abre (Medtronic)	Symptomatic iliofemoral venousoutflow obstruction	Open-cell design with 3 points of connection between cells	10–20	40–150	457–711	[161–163]

[2]E-Luminexx is an electropolished version of Luminexx [190]
[3]Reports of stent migration after implantation [191]

is mostly made of Elgiloy (a cobalt alloy) rather than NiTi. This exception was done since, according to [133,146], Wallstent is one of the most important SX stents used in venous surgery, and it is also frequently employed off-label for both arterial and venous applications. In Table 6, *d*, *l*, and *t*, respectively, represent the diameter, length, and strut thickness of the stents.

Regarding the dimensions of the venous stents, it is important to note that the average size of the blood vessels in the venous system is larger than those in the arterial system. As a result, venous stents have larger diameters compared to arterial stents. This can be observed in Table 4 and Table 6, where the average maximum diameter of arterial stents is approximately 9 mm, while the corresponding number for venous stents is around 20 mm. The same consideration can be made for the strut thickness, which for arterial stents is almost less than 200 microns, while in the case of venous stents, the thickness is mostly about 300 microns, with the exception of the ABRE stent, which is significantly larger than the others. The motivation is due to the larger vessels (in general veins are larger than the arteries) and the fact that the elastic modulus of the vein is much lower than arteries reducing the need to flexibility and the risk of restenosis [147]. It should be noted that some designs of venous stents can also be adapted for arterial applications, however with different sizes in dimensions, including diameter, length, and thickness. In other words this kind of stents are off-label stents, such as Zilver design which is utilized for both venous and arterial stents with corresponding modifications to diameter, length, and thickness, as seen in Table 6.

Mechanical parameters are a focal point of investigation in numerous research studies. Table 7 provides a concise summary of findings from various studies exploring these parameters including, RRF, COF, CR, foreshortening and radial stiffness.

In 2023, Ningcheng Li et al. [167], conducted a study *in-vitro* focusing on the crush resistance and coaxial deployment of a SX NiTi venous stent, Venovo (Bard), and a BX stent (Palmaz XL). In 2021, Masud Hejazi et al. [77,168], compared four different SX commercial stents currently being used in practice for venous stenting, Zilver Vena (Chevron design, NiTi), Luminexx (Diamond design, NiTi), Cook Z (Z design, stainless steel) and Wallstent (braided design, stainless steel). They compared the deformation characteristics of all four designs by examining radial compliance, radial pressure exerted by the stent on veins, and foreshortening through *in-vivo* experiments coupled with analytical and finite element methods. Although, this investigation was done at different stent OS, part of their findings is summarized in Table 7 at a 30 % OS because the normal range for SX stent oversizing is between 20 % and 40 % [82,83]. Dabir et al. [88] investigated seven large lumen stents: Zilver Vena, Sinus XL Flex, Venovo, Sinus Venous, Vici, Sinus Obliquus, and Wallstent. All stents were in NiTi and made by laser-cut

Table 7
Comparison of commercial SX venous stents: mechanical properties.

SX venous stents	Open-cell, NiTi						Closed-cell, NiTi		Hybrid-cell, NiTi	Braided, Elgiloy
	Zilver Vena	Sinus XL Flex	Luminexx	Venovo	Sinus Venous	AbreVenous	Sinus XL	Vici	Sinus Obliquus	Wallstent
RRF (N/mm)	0.67 [88]	1.27 [88]	N.A.	1.65 [88]	1.88 [88]	0.079–0.403 [162]	0.16 [88]	1.11 [88]	1.94 [88]	0.39 [88]
COF at 50 % diameter (N/mm)	0.34 [88]	0.54 [88]	N.A.	0.73 [88]	0.75 [88]	More than 0.026 [162]	N.A.	0.33 [88]	0.79 [88]	0.21 [88]
CR at 50 % diameter (N/mm)	0.054 [88]	0.085 [88]	0.27 [77]	0.076 [88] 0.131 [167]	0.095 [88]	N.A.	N.A.	0.089 [88]	0.141 [88]	0.130 [88]
Foreshortening at 30 % OS (%)	2.5 [77] Minimal [169]	N.A.	8 [77]	Minimal [86]	N.A.	Less than 10 [162]	Almost zero [154]	Less than 20 [158]	N.A.	Substantial, up to 40 [86,150,170]
Radial stiffness at 30 % oversizing (kPa)	0.66 [77]	N.A.	0.16 [77]	N.A.	N.A.	0.007–2.94 [162]	N.A.	N.A.	N.A.	N.A.

technique. The investigated stents were all 14 mm in diameter and ranged from 60 to 120 mm in length. The result of the RRF, COF and CR of all the stents are also presented in Table 7. The values of forces were normalized by dividing them by the corresponding stent length, facilitating direct comparison between different stents.

From Table 7, it is evident that, as expected, each stent design exhibits a higher value of RRF compared to its corresponding COF. The RRF, COF, and CR values among the listed venous stents vary significantly and are dependent upon the specific stent designs. Notably, the Sinus Obliquus stent with its hybrid-cell design demonstrates the highest radial forces (RRF and COF) due to its unique structural design, particularly the presence of closed-cell segments at both ends. Although having enough COF in the Sinus Obliquus can be an advantage for adequate expansion in the vessel, it is worth noting that its elevated COF could potentially raise the risk of restenosis. Foreshortening, as emphasized before, is pivotal for precise stent positioning, with Sinus XL, Venovo, and Zilver Vena exhibiting optimal values in this regard, thereby facilitating deployment. Conversely, the Wallstent design undergoes considerable reduction post-deployment, attributed to its spring-like behavior, where interwoven wires can easily slide against each other.

To summarize, Section 4 of this review was devoted to the analysis of some commercial arterial and venous SX NiTi endovascular stents. This comparison is certainly not complete, as the range of endovascular stents on the market is enormous and constantly evolving. However, it is intended to serve as a guide for stent designers, experts and stakeholders in understanding and evaluating some of the engineering features of endovascular stents and in their selection.

5. Ongoing trends in stents design

Cardiovascular disease remains a formidable global health challenge, contributing significantly to morbidity and mortality worldwide. Although stenting is an effective way to treat cardiovascular disease, the clinical reports reveal that there are still some issues such as vessel recoiling and stents migration post-deployment, fracture, and in-stent restenosis. Furthermore, the scarce presence of commercial stents suitable for deployment into some complex anatomy districts (bifurcations, diameter variation, and so on) exacerbates the challenges in cardiovascular intervention, where it falls upon the surgeon to choose one or more than one stent to meet the specific clinical needs of the patient [171]. Moreover, the inherent anatomical diversity among patients further complicates stent selection, adding another layer of complexity to treatment strategies. Thus, studying the design of an optimum stent that can mitigate these limitations is still a hot topic both for researchers and companies, aiming to enhance treatment efficacy and patients' health. Scholars devoted a strong effort on improving biocompatibility, reducing failure rates, and enhancing the performance of stents through advanced materials, optimum cell-design, and manufacturing techniques. Therefore, biodegradable stents are a significant trend nowadays [172–175], as they boast exceptional biocompatibility that plays a pivotal role in their rising popularity. They are designed to provide temporary support tissue growth before dissolving completely, thereby minimizing long-term complications. This evolution addresses the limitations inherent in durable polymer-based conventional drug-eluting stents, which raise the risk of in-stent restenosis and stent thrombosis by causing neoatherosclerosis and chronic local inflammation [176]. On the design and technology side, there is a growing interest in using additive manufacturing (AM) techniques to manufacture stents. AM has emerged as a prominent trend in recent years, evident from the increasing number of publications on AM of different stents either BMS or BDS [52,56,172,177–181]. This trend signifies a fundamental shift in stent manufacturing methodologies, particularly in response to the limitations associated with conventional manufacturing processes such as laser-cutting. For instance, the dimensions of the stents that are conventionally manufactured by laser cutting from tubes, are dependent on available tubes, limiting dimensional selection of the stent. The available tube diameters may not perfectly match the ideal diameter needed for a particular patient's anatomy, forcing the surgeons to select a stent with a diameter slightly larger than necessary to ensure that it fits properly within the blood vessel, which can lead to negative clinical consequences, such as thrombosis and restenosis [55]. While considering AM, the design and manufacture of patient-specific stents, that precisely conform to individual vascular dimensions, is now possible and has started becoming more popular recently [182,183]. Moreover, AM can deal with complex geometries such as vessel bifurcations, which are typical of many regions in the vascular system. This approach has been recently investigated in technical literature [184] but AM in general offers a solution for creating and manufacturing complex geometries and cell designs. The freedom of shape given by AM has recently motivated designers to explore and analyze more complex geometries such as auxetic structures [185–187] to enhance mechanical properties and overall performance of stents.

The increasing use of AM opens the need for the designer to move from the current state of the art, largely based on laser-cut tubes and investigate new shapes and geometry, which is why the collection of dimensions and the definition of figures of merit is fundamental for the next generation of stents. The comparative tables reported in this review show that the solutions could be very different in terms of strut size, cell shape and design, and on top of this, strong improvements can be envisioned mainly relying on possible customization of these products based on computed tomography (CT) scans of patients. The use of new emerging technologies not only allows the designers to achieve the best tradeoff between the several figures of merit of the endovascular NiTi SX stents, but also opens new possibilities in terms of optimization of the geometry based on methods such as generative design and topological optimization [30,185,188,189].

In summary, the current trends in stent design and manufacturing reflect a significant shift towards addressing the limitations and challenges faced in cardiovascular interventions. Researchers are increasingly focusing on enhancing biocompatibility and improving stent performance through the use of advanced materials, optimal cell designs, and innovative manufacturing techniques such as AM. This work, providing a quantitative insight of the geometry, the dimension, and the mechanical properties of many commercial stents both for arterial and venous applications along with a detailed description of the main figures of merit of the stents, will help the future stent designers in exploiting new possibilities such as AM to improve the performance of these devices and enhance the global health.

6. Conclusion

Endovascular stents are widely used to treat one of the most severe causes of vessel pathologies, the atherosclerotic vascular disease without the use of conventional open surgery, which is one of the motivations behind the rapid diffusion of these devices in the last 20 years. Focusing on SX NiTi stents, a variety of different designs can be traced in the market. Most stents exploit a hybrid design, tend to be very compliant in bending and to provide low force on the vessel's walls, preventing inflammation while maintaining patency. The aim of this review work is to set a solid foundation for the stent designer by providing a solid foundation on which new technical specifications can be built. This purpose is achieved by comparing commercial devices and by listing the main figures of merit of a stent, including the factors affecting fatigue life and mechanical stress on the stent. This overview should be useful both for the mechanical stent designers of the future and for the thoughtful selection of the actual devices, typically done by clinicians. Since the laser-cutting technology was one the strongest limitations in stent design and the AM emerges as a very rapidly advancing substitute, this review provides a quantitative and solid baseline for the future devices design and development, opening the path for the ideal stent, both considering feasibility and performance.

Funding

The support of the MUR project Next Generation EU PRIN 20228AZTYB - GIFTED (desiGn of addItive manuFactured niTinol Endovascular Devices) is gratefully acknowledge.

CRediT authorship contribution statement

Farzaneh Hoseini: Methodology, Formal analysis, Investigation, Writing – original draft, Writing – review & editing, Visualization. **Alberto Bellelli:** Methodology, Formal analysis, Investigation, Writing – original draft, Writing – review & editing, Visualization. **Luke Mizzi:** Data curation, Supervision. **Felice Pecoraro:** Validation, Funding acquisition. **Andrea Spaggiari:** Conceptualization, Methodology, Formal analysis, Investigation, Data curation, Writing – original draft, Writing – review & editing, Supervision, Project administration, Funding acquisition.

Declaration of Competing Interest

The authors declare that they have no known competing financial interests or personal relationships that could have appeared to influence the work reported in this paper.

Acknowledgements

We thank Dott. Nicola Tusini and Dott. Antonio Fontana from Vascular Surgery, AO Reggio Emilia, Arcispedale S. Maria Nuova, Reggio Emilia, Italy, for the fruitful discussion and assistance with the stenting medical procedure. We also would like to thank Dott. Elisa Paini for comments that greatly improved the manuscript and for her enthusiasm.

Data Availability

Data will be made available on request.

References

[1] S.Q. Khan, P.F. Ludman, Percutaneous coronary intervention, Medicine 50 (2022) 437–444, https://doi.org/10.1016/j.mpmed.2022.04.008.
[2] H. Bjarnason, Venoplasty and Stenting. in: Handbook of Angioplasty and Stenting Procedures, Springer London, 2010, pp. 303–315, https://doi.org/10.1007/978-1-84800-399-6_23.
[3] A. Desyatova, W. Poulson, P. Deegan, C. Lomneth, A. Seas, K. Maleckis, J. MacTaggart, A. Kamenskiy, Limb flexion-induced twist and associated intramural stresses in the human femoropopliteal artery, J. R. Soc. Interface 14 (2017), https://doi.org/10.1098/rsif.2017.0025.
[4] C.T. Dotter, Transluminally-placed coilspring endarterial tube grafts, Invest Radio. 4 (1969) 329–332.
[5] C.T. Dotter, R.W. Buschmann, K. Montgomery, McKiNney, Rösch Josef, Transluminal expandable nitinol coil stent grafting: preliminary report, Radiology 147 (1983) 259–260.
[6] M.M. Payne, Charles Theodore Dotter - The father of intervention, Historical Perspectives (2001).
[7] F. Ahadi, M. Azadi, M. Biglari, M. Bodaghi, A. Khaleghian, Evaluation of coronary stents: a review of types, materials, processing techniques, design, and problems, Heliyon 9 (2023) e13575, https://doi.org/10.1016/J.HELIYON.2023.E13575.
[8] C. Pan, Y. Han, J. Lu, Structural design of vascular stents: a review, Micro (Basel) 12 (2021), https://doi.org/10.3390/mi12070770.
[9] C. McCormick, Overview of Cardiovascular Stent Designs. in: Functionalised Cardiovascular Stents, Elsevier, 2017, pp. 3–26, https://doi.org/10.1016/B978-0-08-100496-8.00001-9.
[10] A. Kapoor, N. Jepson, N.W. Bressloff, P.H. Loh, T. Ray, S. Beier, The road to the ideal stent: a review of stent design optimisation methods, findings, and opportunities, Mater. Des. 237 (2024) 112556, https://doi.org/10.1016/J.MATDES.2023.112556.
[11] M.S. Lee, G. Banka, In-stent restenosis, Inter. Cardiol. Clin. 5 (2016) 211–220, https://doi.org/10.1016/J.ICCL.2015.12.006.
[12] S.H. Im, D.H. Im, S.J. Park, Y. Jung, D.H. Kim, S.H. Kim, Current status and future direction of metallic and polymeric materials for advanced vascular stents, Prog. Mater. Sci. 126 (2022), https://doi.org/10.1016/j.pmatsci.2022.100922.
[13] G. Tepe, R. Bantleon, K. Brechtel, J. Schmehl, T. Zeller, C.D. Claussen, F.F. Strobl, Management of peripheral arterial interventions with mono or dual antiplatelet therapy-the MIRROR study: A randomised and double-blinded clinical trial, Eur Radiol 22 (2012) 1998-2006. https://doi.org/10.1007/S00330-012-2441-2/TABLES/5.
[14] P.J. Geraghty, M.W. Mewissen, M.R. Jaff, G.M. Ansel, Three-year results of the VIBRANT trial of VIABAHN endoprosthesis versus bare nitinol stent implantation for complex superficial femoral artery occlusive disease, J. Vasc. Surg. 58 (2013) 386–395.e4, https://doi.org/10.1016/J.JVS.2013.01.050.
[15] K. Miki, K. Fujii, M. Fukunaga, D. Kawasaki, M. Shibuya, T. Imanaka, H. Tamaru, M. Masutani, M. Ohyanagi, T. Masuyama, Impact of post-procedural intravascular ultrasound findings on long-term results following self-expanding nitinol stenting in superficial femoral artery lesions, Circ. J. 77 (2013) 1543–1550, https://doi.org/10.1253/CIRCJ.CJ-12-1182.
[16] F. Pecoraro, E. Dinoto, D. Pakeliani, D. Mirabella, F. Ferlito, G. Bajardi, Efficacy and one-year outcomes of Luminor® paclitaxel-coated drug-eluting balloon in the treatment of popliteal artery atherosclerosis lesions, Ann. Vasc. Surg. 76 (2021) 370–377, https://doi.org/10.1016/J.AVSG.2021.04.015.
[17] D. Scheinert, S. Scheinert, J. Sax, C. Piorkowski, S. Bräunlich, M. Ulrich, G. Biamino, A. Schmidt, Prevalence and clinical impact of stent fractures after femoropopliteal stenting, J. Am. Coll. Cardiol. 45 (2005) 312–315, https://doi.org/10.1016/J.JACC.2004.11.026.
[18] M. Intaglietta, Vasomotion and flowmotion: physiological mechanisms and clinical evidence, Vasc. Med. Rev. 1 (1990) 101–112.
[19] Y. Sotomi, Y. Onuma, C. Collet, E. Tenekecioglu, R. Virmani, N.S. Kleiman, P. W. Serruys, Bioresorbable scaffold - the emerging reality and future directions, Circ. Res 120 (2017) 1341–1352, https://doi.org/10.1161/circresaha.117.310275.
[20] A.R. Pelton, V. Schroeder, M.R. Mitchell, X.Y. Gong, M. Barney, S.W. Robertson, Fatigue and durability of Nitinol stents, J. Mech. Behav. Biomed. Mater. 1 (2008) 153–164, https://doi.org/10.1016/J.JMBBM.2007.08.001.
[21] T.W. Duerig, M. Wholey, A comparison of balloon- and self-expanding stents, Minim. Invasive Ther. Allied Technol. 11 (2002) 173–178, https://doi.org/10.1080/136457002760273386.
[22] G. Mani, M.D. Feldman, D. Patel, C.M. Agrawal, Coronary stents: a materials perspective, Biomaterials 28 (2007) 1689–1710, https://doi.org/10.1016/J.BIOMATERIALS.2006.11.042.
[23] A. Firoozi, B. Mohebbi, F. Noohi, H. Bassiri, A. Mohebbi, S. Abdi, M. Maleki, O. Shafe, M.M. Peighambari, M.J. Alemzadeh-Ansari, H. Bakhshandeh, Y. Rezaei, N. Sepehrvand, Self-expanding versus balloon-expandable stents in patients with isthmic coarctation of the aorta, Am. J. Cardiol. 122 (2018) 1062–1067, https://doi.org/10.1016/J.AMJCARD.2018.06.005.
[24] R. He, L.G. Zhao, V.V. Silberschmidt, H. Willcock, A computational study of fatigue resistance of nitinol stents subjected to walk-induced femoropopliteal artery motion, J. Biomech. 118 (2021) 110295, https://doi.org/10.1016/J.JBIOMECH.2021.110295.
[25] I. Avdeev, M. Shams, Vascular Stents: Coupling full 3-D With Reduced-Order Structural Models. in: IOP Conf Ser Mater Sci Eng, Institute of Physics Publishing, 2014, https://doi.org/10.1088/1757-899X/10/1/012133.
[26] A.R. Saraf, S.P. Yadav, Fundamentals of bare-metal stents, Elsevier Ltd, 2017, https://doi.org/10.1016/B978-0-08-100496-8.00002-0.
[27] T. Hanawa, Materials for metallic stents, J. Artif. Organs 12 (2009) 73–79, https://doi.org/10.1007/s10047-008-0456-x.
[28] R.B. Heimann, Materials for medical application, Materials for Medical Application (2020) 1-615. https://doi.org/10.1515/9783110619249.
[29] C. Shanahan, P. Tiernan, S.A.M. Tofail, Looped ends versus open ends braided stent: a comparison of the mechanical behaviour using analytical and numerical methods, J. Mech. Behav. Biomed. Mater. 75 (2017) 581–591, https://doi.org/10.1016/J.JMBBM.2017.08.025.
[30] S.F. Hoseini, A. Spaggiari, Design and optimization of a self-expandable niti braided stent using MOPSO algorithm, X ECCOMAS thematic conference on smart structures and materials, SMART 2023 (2023) 454–464, https://doi.org/10.7712/150123.9800.449429.
[31] N. Sabahi, W. Chen, C.H. Wang, J.J. Kruzic, X. Li, A review on additive manufacturing of shape-memory materials for biomedical applications, JOM 72 (2020) 1229–1253, https://doi.org/10.1007/S11837-020-04013-X/FIGURES/13.
[32] D. Stoeckel, A. Pelton, T. Duerig, Self-expanding nitinol stents: material and design considerations, Eur. Radio. 14 (2004) 292–301, https://doi.org/10.1007/s00330-003-2022-5.
[33] S.F. Hoseini, S.A. MirMohammadSadeghi, A. Fathi, H.M. Daniali, Adaptive predictive control of a novel shape memory alloy rod actuator, Proc. Inst. Mech. Eng. Part I: J. Syst. Control Eng. 235 (2021) 291–301, https://doi.org/10.1177/0959651820974488.
[34] B. He, X. Dong, R. Nie, Y. Wang, S. Ao, G. Wang, Comprehensive shape memory alloys constitutive models for engineering application, Mater. Des. 225 (2023) 111563, https://doi.org/10.1016/J.MATDES.2022.111563.
[35] A. Tuissi, S. Carr, J. Butler, A.A. Gandhi, L. O'Donoghue, K. McNamara, J. M. Carlson, S. Lavelle, P. Tiernan, C.A. Biffi, P. Bassani, S.A.M. Tofail, Radiopaque shape memory alloys: NiTi–Er with stable superelasticity, Shape Mem. Superelasticity 2 (2016) 196–203, https://doi.org/10.1007/s40830-016-0066-z.
[36] B. Lin, K. Gall, H.J. Maier, R. Waldron, Structure and thermomechanical behavior of NiTiPt shape memory alloy wires, Acta Biomater. 5 (2009) 257–267, https://doi.org/10.1016/j.actbio.2008.07.015.
[37] J.-S. Park, K.H. Yim, S. Jeong, D.H. Lee, D.G. Kim, A novel high-visibility radiopaque tantalum marker for biliary self-expandable metal stents, Gut Liver 13 (2019) 366–372, https://doi.org/10.5009/gnl18330.

[38] S. Alipour, F. Taromian, E.R. Ghomi, M. Zare, S. Singh, S. Ramakrishna, Nitinol: From historical milestones to functional properties and biomedical applications, Proc. Inst. Mech. Eng. H. 236 (2022) 1595–1612, https://doi.org/10.1177/09544119221123176.
[39] K. Maleckis, E. Anttila, P. Aylward, W. Poulson, A. Desyatova, J. MacTaggart, A. Kamenskiy, Nitinol stents in the femoropopliteal artery: a mechanical perspective on material, design, and performance, Ann. Biomed. Eng. 46 (2018) 684–704, https://doi.org/10.1007/s10439-018-1990-1.
[40] M. Elahinia, N. Shayesteh Moghaddam, M. Taheri Andani, A. Amerinatanzi, B. A. Bimber, R.F. Hamilton, Fabrication of NiTi through additive manufacturing: a review, Prog. Mater. Sci. 83 (2016) 630–663, https://doi.org/10.1016/J.PMATSCI.2016.08.001.
[41] A. Solis Eichler, Mechanical and Material Properties of Nitinol and its Application to Stents, Master's degree thesis, Florida Institute of Technology, 2020. ⟨https://repository.fit.edu/etd⟩.
[42] S.W. Robertson, On the mechanical properties and microstructure of Nitinol for biomedical stent applications, PhD thesis, University of California, Berkeley, 2006.
[43] A. Bramucci, A. Fontana, C.B. Massoni, E. Vecchiati, A. Freyrie, N. Tusini, Dual- vs single-layer stents for endovascular treatment of symptomatic and asymptomatic internal carotid artery stenosis, Cardiovasc. Revascularization Med. 57 (2023) 34–40, https://doi.org/10.1016/J.CARREV.2023.06.016.
[44] S. Lilburn, P.K. Norton, M. Zupkofska, L. Bedard, G.D. Harding, Atraumatic stent and method and apparatus for making the same, 2009. ⟨http://www.patentbuddy.com/Patent/8151682⟩.
[45] StarCut Tube - CNC Laser Cutting Machine | Coherent, (2024). ⟨https://www.coherent.com/machines-systems/laser-cutting-drilling/starcut-tube⟩ (accessed May 17, 2024).
[46] 3D Printed Nitinol Opens New Possibilities for Arterial Stents | Additive Manufacturing, (2020). ⟨https://www.additivemanufacturing.media/articles/3d-printed-nitinol-opens-new-possibilities-for-arterial-stents⟩ (accessed May 2, 2024).
[47] S. Salamaga, H. Stępak, M. Żołyński, J. Kaczmarek, M. Błaszyk, M.G. Staniśić, Z. Krasiński, Three-year real-world outcomes of interwoven nitinol supera stent implantation in long and complex femoropopliteal Lesions, J. Clin. Med 12 (2023), https://doi.org/10.3390/jcm12144869.
[48] K. Maleckis, P. Deegan, W. Poulson, C. Sievers, A. Desyatova, J. MacTaggart, A. Kamenskiy, Comparison of femoropopliteal artery stents under axial and radial compression, axial tension, bending, and torsion deformations, J. Mech. Behav. Biomed. Mater. 75 (2017) 160–168, https://doi.org/10.1016/j.jmbbm.2017.07.017.
[49] A.G. Demir, B. Previtali, Lasers in the manufacturing of cardiovascular metallic stents: subtractive and additive processes with a digital tool, : Procedia Comput. Sci., Elsevier B. V. (2022) 604–613, https://doi.org/10.1016/j.procs.2022.12.256.
[50] L. Yan, S.L. Soh, N. Wang, Q. Ma, W.F. Lu, S.T. Dheen, A.S. Kumar, J.Y.H. Fuh, Evaluation and characterization of nitinol stents produced by selective laser melting with various process parameters, Prog. Addit. Manuf. 7 (2022) 1141–1153, https://doi.org/10.1007/s40964-022-00289-4.
[51] V. Finazzi, F. Berti, L. Petrini, B. Previtali, A.G. Demir, Additive manufacturing and post-processing of superelastic NiTi micro struts as building blocks for cardiovascular stents, Addit. Manuf. 70 (2023) 103561, https://doi.org/10.1016/J.ADDMA.2023.103561.
[52] Y. Li, Y. Shi, Y. Lu, X. Li, J. Zhou, A.A. Zadpoor, L. Wang, Additive manufacturing of vascular stents, Acta Biomater. 167 (2023) 16–37, https://doi.org/10.1016/J.ACTBIO.2023.06.014.
[53] H. Meier, C. Haberland, J. Frenzel, Structural and functional properties of NiTi shape memory alloys produced by Selective Laser Melting, in: 2011. https://doi.org/10.1201/B11341-47.
[54] V. Finazzi, F. Berti, R.J. Guillory, L. Petrini, B. Previtali, A.G. Demir, Patient-specific cardiovascular superelastic NiTi stents produced by laser powder bed fusion, : Procedia CIRP, Elsevier B. V. (2022) 244–248, https://doi.org/10.1016/j.procir.2022.06.044.
[55] O.M. McGee, S. Geraghty, C. Hughes, P. Jamshidi, D.P. Kenny, M.M. Attallah, C. Lally, An investigation into patient-specific 3D printed titanium stents and the use of etching to overcome Selective Laser Melting Design Constraints, J. Mech. Behav. Biomed. Mater. 134 (2022) 105388, https://doi.org/10.1016/J.JMBBM.2022.105388.
[56] P. Jamshidi, C. Panwisawas, E. Langi, S.C. Cox, J. Feng, L. Zhao, M.M. Attallah, Development, characterisation, and modelling of processability of nitinol stents using laser powder bed fusion, J. Alloy. Compd. 909 (2022) 164681, https://doi.org/10.1016/J.JALLCOM.2022.164681.
[57] M.A. Obeidi, A.R. Al-Hamaoy, A. Cholkar, N. Agarwal, D. Brabazon, Comparing the surface characteristics of additively manufactured nitinol parts polished by femto-second and CO2 laser, Appl. Surf. Sci. Adv. (2024) 100637, https://doi.org/10.1016/j.apsadv.2024.100637.
[58] J. Dong, M. Pacella, Y. Liu, L. Zhao, Surface engineering and the application of laser-based processes to stents - a review of the latest development, Bioact. Mater. 10 (2022) 159–184, https://doi.org/10.1016/J.BIOACTMAT.2021.08.023.
[59] A. Lantada, C. Vega, R. Martínez, M. Rendón, M. Li, Ó. Contreras-Almengor, J. Ordoño, W. Solórzano-Requejo, M. Vasic, J. Munoz-Guijosa, J. Molina-Aldareguia, Additive manufacturing of nitinol for smart personalized medical devices: current capabilities and challenges, : Scitepress (2024) 123–134, https://doi.org/10.5220/0012363900003657.
[60] A.M. Sousa, A.M. Amaro, A.P. Piedade, 3D printing of polymeric bioresorbable stents: a strategy to improve both cellular compatibility and mechanical properties, Polymers 2022 (2022) 1099, https://doi.org/10.3390/polym.
[61] M. Somireddy, A. Czekanski, Anisotropic material behavior of 3D printed composite structures – material extrusion additive manufacturing, Mater. Des. 195 (2020) 108953, https://doi.org/10.1016/J.MATDES.2020.108953.
[62] S. Dadbakhsh, B. Vrancken, J.P. Kruth, J. Luyten, J. Van Humbeeck, Texture and anisotropy in selective laser melting of NiTi alloy, Mater. Sci. Eng.: A 650 (2016) 225–232, https://doi.org/10.1016/J.MSEA.2015.10.032.
[63] Vascular Stents Market Size, Trends, Forecast Report 2032, IMARC (2024). ⟨https://www.imarcgroup.com/vascular-stents-market⟩ (accessed August 23, 2024).
[64] Guidance for Industry and FDA Staff, Non-Clinical Engineering Tests and Recommended Labeling for Intravascular Stents and Associated Delivery Systems, 2010. ⟨http://www.fda.gov/MedicalDevices/DeviceRegulationandGuidance/GuidanceDocuments/ucm0⟩.
[65] D.E. Kiousis, A.R. Wulff, G.A. Holzapfel, Experimental studies and numerical analysis of the inflation and interaction of vascular balloon catheter-stent systems, Ann. Biomed. Eng. 37 (2009) 315–330, https://doi.org/10.1007/s10439-008-9606-9.
[66] A.G. Verstandig, A.I. Bloom, T. Sasson, Y.S. Haviv, D. Rubinger, Shortening and migration of Wallstents after stenting of central venous stenoses in hemodialysis patients, Cardiovasc Interv. Radio. 26 (2003) 58–64, https://doi.org/10.1007/S00270-002-1953-6/METRICS.
[67] P.K.M. Prithipaul, M. Kokkolaras, D. Pasini, Assessment of structural and hemodynamic performance of vascular stents modelled as periodic lattices, Med Eng. Phys. 57 (2018) 11–18, https://doi.org/10.1016/J.MEDENGPHY.2018.04.017.
[68] R. Improta, P. Scarparo, J. Wilschut, Q. Wolff, J. Daemen, W.K. Den Dekker, F. Zijlstra, N.M. Van Mieghem, R. Diletti, Elastic stent recoil in coronary total occlusions: Comparison of durable-polymer zotarolimus eluting stent and ultrathin strut bioabsorbable-polymer sirolimus eluting stent, Catheter. Cardiovasc. Interv. 99 (2022) 88–97, https://doi.org/10.1002/ccd.29739.
[69] N.C. Liu, Robust optimisation of Coronary Stents, PhD thesis, The University of Sydney, 2022.
[70] L. Wiesent, U. Schultheiß, C. Schmid, T. Schratzenstaller, A. Nonn, Experimentally validated simulation of coronary stents considering different dogboning ratios and asymmetric stent positioning, PLoS One 14 (2019), https://doi.org/10.1371/journal.pone.0224026.
[71] M.R. Jedwab, C.O. Clerc, A study of the geometrical and mechanical properties of a self-expanding metallic stent–theory and experiment, J. Appl. Biomater. 4 (1993) 77–85, https://doi.org/10.1002/jab.770040111.
[72] W. Schmidt, C. Brandt-Wunderlich, P. Behrens, C. Kopetsch, K.P. Schmitz, J. R. Andresen, N. Grabow, Revisiting SFA stent technology: an updated overview on mechanical stent performance, Biomed. Tech. 68 (2023) 523–535, https://doi.org/10.1515/bmt-2022-0412.
[73] M.T. Vote, J.M. Hendriks, J.H.H. Van Laanen, P.M.T. Pattynama, B.E. Muhs, D. Poldermans, H.J.M. Verhagen, Radial force measurements in carotid stents: influence of stent design and length of the Lesion, J. Vasc. Interv. Radiol. 22 (2011) 661–666, https://doi.org/10.1016/J.JVIR.2011.01.450.
[74] E. Dragoni, D. Castagnetti, A. Spaggiari, Lezioni di Costruzione di Macchine, Società Editrice Esculapio, 2023.
[75] D.Bin Kim, H. Choi, S.M. Joo, H.K. Kim, J.H. Shin, M.H. Hwang, J. Choi, D. G. Kim, K.H. Lee, C.H. Lim, S.K. Yoo, H.M. Lee, K. Sun, A comparative reliability and performance study of different stent designs in terms of mechanical properties: foreshortening, recoil, radial force, and flexibility, Artif. Organs 37 (2013) 368–379, https://doi.org/10.1111/aor.12001.
[76] Y. Liu, J. Yang, Y. Zhou, J. Hu, Structure Design of Vascular Stents. in: Multiscale Simulations and Mechanics of Biological Materials, John Wiley and Sons, 2013, pp. 301–317, https://doi.org/10.1002/9781118402955.ch16.
[77] M. Hejazi, F. Sassani, J. Gagnon, Y. Hsiang, A.S. Phani, Deformation mechanics of self-expanding venous stents: modelling and experiments, J. Biomech. 120 (2021) 110333, https://doi.org/10.1016/J.JBIOMECH.2021.110333.
[78] C. Kleinstreuer, Z. Li, C.A. Basciano, S. Seelecke, M.A. Farber, Computational mechanics of nitinol stent grafts, J. Biomech. 41 (2008) 2370–2378, https://doi.org/10.1016/J.JBIOMECH.2008.05.032.
[79] T.W. Tan, G.R. Douglas, T. Bond, A.S. Phani, Compliance and longitudinal strain of cardiovascular stents: influence of cell geometry, J. Med. Devices, Trans. ASME 5 (2011) 1–6, https://doi.org/10.1115/1.4005226.
[80] E.J. Hearn, Mechanics of Materials 1 - An Introduction to the Mechanics of Elastic and Plastic Deformation of Solids and Structural Materials, Butterworth-Heinemann, 1997.
[81] S. Weiß, H. Szymczak, A. Meißner, Fatigue and endurance of coronary stents, Materwiss Werksttech 40 (2009) 61–64, https://doi.org/10.1002/mawe.200800409.
[82] H.Q. Zhao, A. Nikanorov, R. Virmani, R. Jones, E. Pacheco, L.B. Schwartz, Late stent expansion and neointimal proliferation of oversized nitinol stents in peripheral arteries, Cardiovasc Interv. Radio. 32 (2009) 720–726, https://doi.org/10.1007/s00270-009-9601-z.
[83] M. Bernini, M. Colombo, C. Dunlop, R. Hellmuth, C. Chiastra, W. Ronan, T. J. Vaughan, Oversizing of self-expanding Nitinol vascular stents – a biomechanical investigation in the superficial femoral artery, J. Mech. Behav. Biomed. Mater. 132 (2022) 105259, https://doi.org/10.1016/J.JMBBM.2022.105259.
[84] J. van Prehn, F.J.V. Schlösser, B.E. Muhs, H.J.M. Verhagen, F.L. Moll, J.A. van Herwaarden, Oversizing of aortic stent grafts for abdominal aneurysm repair: a

systematic review of the benefits and risks, Eur. J. Vasc. Endovasc. Surg. 38 (2009) 42–53, https://doi.org/10.1016/J.EJVS.2009.03.025.
[85] Y. Qi, C. Weng, D. Yuan, T. Wang, Y. Ma, Y. Yang, J. Zhao, B. Huang, Oversizing consideration of proximal stent graft in hemodynamically stable and unstable patients undergoing emergent endovascular aortic repair, J. Clin. Med 12 (2023) 7500, https://doi.org/10.3390/JCM12237500/S1.
[86] M.A.H. Taha, A. Busuttil, R. Bootun, B.A.H. Thabet, A.E.H. Badawy, H.A. Hassan, J. Shalhoub, A.H. Davies, Clinical outcomes and overview of dedicated venous stents for management of chronic iliocaval and femoral deep venous disease, Vascular 30 (2022) 320–330, https://doi.org/10.1177/1708538121989860.
[87] J.C. Palmaz, Intravascular stents: tissue-stent interactions and design considerations, Am. J. Roentgenol. 160 (1993) 613–618, https://doi.org/10.2214/ajr.160.3.8430566.
[88] D. Dabir, A. Feisst, D. Thomas, J.A. Luetkens, C. Meyer, A. Kardulovic, M. Menne, U. Steinseifer, H.H. Schild, D.L.R. Kuetting, Physical properties of venous stents: an experimental comparison, Cardiovasc Interv. Radio. 41 (2018) 942–950, https://doi.org/10.1007/s00270-018-1916-1.
[89] C. Brandt-Wunderlich, W. Schmidt, N. Grabow, M. Stiehm, S. Siewert, R. Andresen, K.P. Schmitz, Support function of self-expanding nitinol stents - are radial resistive force and crush resistance comparable? : Curr. Dir. Biomed. Eng., Walter De. Gruyter GmbH (2019) 465–467, https://doi.org/10.1515/cdbme-2019-0117.
[90] N.B. Morgan, Medical shape memory alloy applications—the market and its products, Mater. Sci. Eng.: A 378 (2004) 16–23, https://doi.org/10.1016/J.MSEA.2003.10.326.
[91] H.B. Smouse, A. Nikanorov, D. LaFlash, Biomechanical forces in the femoropopliteal arterial segment, Endovasc. Today (2005) 60–66.
[92] J.N. MacTaggart, N.Y. Phillips, C.S. Lomneth, I.I. Pipinos, R. Bowen, B. Timothy Baxter, J. Johanning, G. Matthew Longo, A.S. Desyatova, M.J. Moulton, Y. A. Dzenis, A.V. Kamenskiy, Three-dimensional bending, torsion and axial compression of the femoropopliteal artery during limb flexion, J. Biomech. 47 (2014) 2249–2256, https://doi.org/10.1016/J.JBIOMECH.2014.04.053.
[93] E. Dordoni, A. Meoli, W. Wu, G. Dubini, F. Migliavacca, G. Pennati, L. Petrini, Fatigue behaviour of Nitinol peripheral stents: the role of plaque shape studied with computational structural analyses, Med Eng. Phys. 36 (2014) 842–849, https://doi.org/10.1016/j.medengphy.2014.03.006.
[94] M. Early, D.J. Kelly, The consequences of the mechanical environment of peripheral arteries for nitinol stenting, Med Biol. Eng. Comput. 49 (2011) 1279–1288, https://doi.org/10.1007/s11517-011-0815-2.
[95] H. Cao, M.H. Wu, F. Zhou, R.M. McMeeking, R.O. Ritchie, The influence of mean strain on the high-cycle fatigue of Nitinol with application to medical devices, J. Mech. Phys. Solids 143 (2020) 104057, https://doi.org/10.1016/j.jmps.2020.104057.
[96] M. Pernot, G. Goudot, Noninvasive ultrafast ultrasound for imaging the coronary vasculature and assessing the arterial wall's biomechanics, Biomech. Coron. Atheroscler. Plaque.: Model Patient (2021) 517–528, https://doi.org/10.1016/B978-0-12-817195-0.00022-6.
[97] C. Jenei, E. Balogh, G.T. Szabó, C.A. Dézsi, Z. Kőszegi, Wall shear stress in the development of in-stent restenosis revisited. A critical review of clinical data on shear stress after intracoronary stent implantation, Cardiol. J. 23 (2016) 365–373, https://doi.org/10.5603/CJ.a2016.0047.
[98] A.M. Malek, S.L. Alper, S. Izumo, Hemodynamic shear stress and its role in atherosclerosis, JAMA 282 (1999) 2035–2042, https://doi.org/10.1001/jama.282.21.2035.
[99] A. Cornelissen, F.J. Vogt, The effects of stenting on coronary endothelium from a molecular biological view: Time for improvement? J. Cell Mol. Med 23 (2019) 39–46, https://doi.org/10.1111/jcmm.13936.
[100] M. Sanmartín, J. Goicolea, C. García, J. García, A. Crespo, J. Rodríguez, J. M. Goicolea, Influence of shear stress on in-stent restenosis: in vivo study using 3D reconstruction and computational fluid dynamics, Rev. Española De. Cardiol. ía (Engl. Ed.) 59 (2006) 20–27, https://doi.org/10.1016/s1885-5857(06)60044-3.
[101] J.F. LaDisa, L.E. Olson, I. Guler, D.A. Hettrick, S.H. Audi, J.R. Kersten, D. C. Warltier, P.S. Pagel, Stent design properties and deployment ratio influence indexes of wall shear stress: a three-dimensional computational fluid dynamics investigation within a normal artery, J. Appl. Physiol. 97 (2004) 424–430, https://doi.org/10.1152/japplphysiol.01329.2003.
[102] F. Gijsen, Y. Katagiri, P. Barlis, C. Bourantas, C. Collet, U. Coskun, J. Daemen, J. Dijkstra, E. Edelman, P. Evans, K. Van Der Heiden, R. Hose, B.K. Koo, R. Krams, A. Marsden, F. Migliavacca, Y. Onuma, A. Ooi, E. Poon, H. Samady, P. Stone, K. Takahashi, D. Tang, V. Thondapu, E. Tenekecioglu, L. Timmins, R. Torii, J. Wentzel, P. Serruys, Expert recommendations on the assessment of wall shear stress in human coronary arteries: existing methodologies, technical considerations, and clinical applications, Eur. Heart J. 40 (2019) 3421–3433, https://doi.org/10.1093/EURHEARTJ/EHZ551.
[103] J.F. LaDisa, L.E. Olson, D.A. Hettrick, D.C. Warltier, J.R. Kersten, P.S. Pagel, Axial stent strut angle influences wall shear stress after stent implantation: analysis using 3D computational fluid dynamics models of stent foreshortening, Biomed. Eng. Online 4 (2005) 1–10, https://doi.org/10.1186/1475-925X-4-59.
[104] A. Sakamoto, H. Jinnouchi, S. Torii, R. Virmani, A.V. Finn, Understanding the impact of stent and scaffold material and strut design on coronary artery thrombosis from the basic and clinical points of view, Bioengineering 2018 5 (2018) 71, https://doi.org/10.3390/BIOENGINEERING5030071.
[105] M.J. Grundeken, M.A.M. Beijk, A narrative review of ultrathin-strut drug-eluting stents: the thinner the better? Heart Int 15 (2021) https://doi.org/10.17925/HI.2021.15.2.84.
[106] M.I. Papafaklis, C.V. Bourantas, P.E. Theodorakis, C.S. Katsouras, D.I. Fotiadis, L. K. Michalis, Relationship of shear stress with in-stent restenosis: bare metal stenting and the effect of brachytherapy, Int J. Cardiol. 134 (2009) 25–32, https://doi.org/10.1016/J.IJCARD.2008.02.006.
[107] C. Chiastra, S. Morlacchi, D. Gallo, U. Morbiducci, R. Cárdenes, I. Larrabide, F. Migliavacca, Computational fluid dynamic simulations of image-based stented coronary bifurcation models, J. R. Soc. Interface 10 (2013), https://doi.org/10.1098/rsif.2013.0193.
[108] F. Migliavacca, L. Petrini, M. Colombo, F. Auricchio, R. Pietrabissa, Mechanical behavior of coronary stents investigated through the finite element method, J. Biomech. 35 (2002) 803–811, https://doi.org/10.1016/S0021-9290(02)00033-7.
[109] D. Lim, S.K. Cho, W.P. Park, A. Kristensson, J.Y. Ko, S.T.S. Al-Hassani, H.S. Kim, Suggestion of potential stent design parameters to reduce restenosis risk driven by foreshortening or dogboning due to non-uniform balloon-stent expansion, Ann. Biomed. Eng. 36 (2008) 1118–1129, https://doi.org/10.1007/s10439-008-9504-1.
[110] M. Azaouzi, N. Lebaal, A. Makradi, S. Belouettar, Optimization based simulation of self-expanding Nitinol stent, Mater. Des. 50 (2013) 917–928, https://doi.org/10.1016/J.MATDES.2013.03.012.
[111] J.F. LaDisa, L.E. Olson, R.C. Molthen, D.A. Hettrick, P.F. Pratt, M.D. Hardel, J. R. Kersten, D.C. Warltier, P.S. Pagel, Alterations in wall shear stress predict sites of neointimal hyperplasia after stent implantation in rabbit iliac arteries, Am. J. Physiol. Heart Circ. Physiol. 288 (2005) 2465–2475, https://doi.org/10.1152/ajpheart.01107.2004.
[112] T. Schmidt, J.D. Abbott, Coronary stents: history, design, and construction, J. Clin. Med 7 (2018), https://doi.org/10.3390/jcm7060126.
[113] E. Tatli, A. Tokatli, M.B. Vatan, M.T. Agac, H. Gunduz, R. Akdemir, H. Kilic, Comparison of closed-cell and hybrid-cell stent designs in Carotid artery stenting: clinical and procedural outcomes, Post. w Kardiol. Inter. 13 (2017) 135–141, https://doi.org/10.5114/pwki.2017.67994.
[114] E.E. de Vries, A.J.A. Meershoek, E.J. Vonken, H.M. den Ruijter, J.C. van den Berg, G.J. de Borst, K. Bijuklic, J. Schofer, L. Bonati, M. Bosiers, J. Wauters, G. de Donato, E. Chisci, C. Setacci, D. Doig, R.L. Featherstone, J. Dobson, M.M. Brown, M.K. Eskandari, J. Giri, I.Q. Grunwald, A.L. Kühn, D.K. Han, P.L. Faries, F. Hernandez-Fernandez, G. Parrilla, M. Hornung, H. Sievert, K. Kono, P. Latacz, J. Ledwoch, H. Mudra, G. Maleux, R. Nolz, T. Ohki, M. Piazza, P. Pieniazek, L. Tekieli, D. Radak, S. Tanaskovic, M. Rasiova, G. Simonte, B. Fiorucci, M.W. K. Tietke, G. Ventoruzzo, A meta-analysis of the effect of stent design on clinical and radiologic outcomes of carotid artery stenting, J. Vasc. Surg. 69 (2019) 1952–1961.e1, https://doi.org/10.1016/J.JVS.2018.11.017.
[115] Medtronic - Cristallo Ideale - The 5F HYBRID Stent Deliverable and Secure, (2012). ⟨https://kategorizacia.mzsr.sk/Pomocky/Download/RequestAttachment/47242⟩ (accessed May 17, 2024).
[116] D. Stoeckel, C. Bonsignore, S. Duda, A survey of stent designs, Minim. Invasive Ther. Allied Technol. 11 (2002) 137–147, https://doi.org/10.1080/136457002760273340.
[117] A. Brambilla, G. Pennati, L. Petrini, F. Berti, Stents in congenital heart disease: state of the art and future scenarios, Appl. Sci. 13 (2023), https://doi.org/10.3390/app13179692.
[118] F. Auricchio, M. Conti, M. Ferraro, A. Reali, Evaluation of carotid stent scaffolding through patient-specific finite element analysis, Int J. Numer. Method Biomed. Eng. 28 (2012) 1043–1055, https://doi.org/10.1002/cnm.2509.
[119] D.S. Pierce, E.B. Rosero, J.G. Modrall, B. Adams-Huet, R.J. Valentine, G. P. Clagett, C.H. Timaran, Open-cell versus closed-cell stent design differences in blood flow velocities after carotid stenting, J. Vasc. Surg. 49 (2009) 602–606, https://doi.org/10.1016/J.JVS.2008.10.016.
[120] M. Conti, D. Van Loo, F. Auricchio, M. De Beule, G. De Santis, B. Verhegghe, S. Pirrelli, A. Odero, Impact of carotid stent cell design on vessel scaffolding: a case study comparing experimental investigation and numerical simulations, J. Endovasc. Ther. 18 (2011) 397–406, https://doi.org/10.1583/10-3338.1.
[121] sinus-XL Stent | Duomed, (2024). ⟨https://www.duomed.com/en-BE/products/sinus-xl-stent⟩ (accessed May 17, 2024).
[122] Biotronik Pulsar-18 brochure, (2024). ⟨https://www.biotronik.com/en-us/products/vi/peripheral/pulsar-18⟩ (accessed May 17, 2024).
[123] L. Wei, Q. Chen, Z. Li, Study on the impact of straight stents on arteries with different curvatures, J. Mech. Med Biol. 16 (2016) 1–13, https://doi.org/10.1142/S0219519416500937.
[124] B.Y.M. Werner, Factors affecting reduction in SFA stent fracture rates, Endovasc. Today 13 (2014) 93–95.
[125] C. Briguori, C. Sarais, P. Pagnotta, F. Liistro, M. Montorfano, A. Chieffo, F. Sgura, N. Corvaja, R. Albiero, G. Stankovic, C. Toutoutzas, E. Bonizzoni, C. Di Mario, A. Colombo, In-stent restenosis in small coronary arteries:impact of strut thickness, J. Am. Coll. Cardiol. 40 (2002) 403–409, https://doi.org/10.1016/S0735-1097(02)01989-7.
[126] A. Kastrati, J. Mehilli, J. Dirschinger, F. Dotzer, H. Schühlen, F.-J. Neumann, M. Fleckenstein, C. Pfafferott, M. Seyfarth, A. Schömig, Intracoronary stenting and angiographic results, Circulation 103 (2001) 2816–2821, https://doi.org/10.1161/01.CIR.103.23.2816.
[127] N. Foin, R.D. Lee, R. Torii, J.L. Guitierrez-Chico, A. Mattesini, S. Nijjer, S. Sen, R. Petraco, J.E. Davies, C. Di Mario, M. Joner, R. Virmani, P. Wong, Impact of stent strut design in metallic stents and biodegradable scaffolds, Int J. Cardiol. 177 (2014) 800–808, https://doi.org/10.1016/J.IJCARD.2014.09.143.
[128] M.M. Torki, S. Hassanajili, M.M. Jalisi, Design optimizations of PLA stent structure by FEM and investigating its function in a simulated plaque artery,

Math. Comput. Simul. 169 (2020) 103–116, https://doi.org/10.1016/J.MATCOM.2019.09.011.
[129] H.M. Hsiao, Y.P. Wang, C.Y. Ko, Y.H. Cheng, H.Y. Lee, A novel nitinol spherical occlusion device for liver cancer, Materials 9 (2016), https://doi.org/10.3390/ma9010019.
[130] C. Bonsignore, Open Stent Design, 2011. https://doi.org/10.6084/M9.FIGSHARE.95614.
[131] E. Masoumi Khalil Abad, D. Pasini, R. Cecere, Shape optimization of stress concentration-free lattice for self-expandable nitinol stent-grafts, J. Biomech. 45 (2012) 1028–1035, https://doi.org/10.1016/J.JBIOMECH.2012.01.002.
[132] S. Barati, N. Fatouraee, M. Nabaei, F. Berti, L. Petrini, F. Migliavacca, J. F. Rodriguez Matas, A computational optimization study of a self-expandable transcatheter aortic valve, Comput. Biol. Med 139 (2021) 104942, https://doi.org/10.1016/J.COMPBIOMED.2021.104942.
[133] I. Massi, P. Zamboni, What are the ideal characteristics of a venous stent? Veins Lymphat. 10 (2021) https://doi.org/10.4081/vl.2021.9739.
[134] A. Schwein, Y. Georg, A. Lejay, P. Nicolini, O. Hartung, D. Contassot, F. Thaveau, F. Heim, N. Chakfe, Endovascular treatment for venous diseases: where are the venous stents? Methodist Debakey Cardiovasc J. (2018) https://doi.org/10.14797/mdcj-14-3-208.
[135] GORE® TIGRIS® Vascular Stent | Gore Medical Europe, (2024). ⟨https://www.goremedical.com/eu/products/tigris⟩ (accessed May 17, 2024).
[136] R. Lorbeer, A. Grotz, M. Dörr, H. Völzke, W. Lieb, J.-P. Kühn, B. Mensel, Reference values of vessel diameters, stenosis prevalence, and arterial variations of the lower limb arteries in a male population sample using contrast-enhanced MR angiography, PLoS One 13 (2018) e0197559, https://doi.org/10.1371/journal.pone.0197559.
[137] Zilver 635® Vascular Self-Expanding Stent | Cook Medical, (2024). ⟨https://www.cookmedical.com/products/di_ziv_635_webds/⟩ (accessed May 17, 2024).
[138] Cordis S.M.A.R.T. - The Stent With the Stats, 2023. ⟨https://cordis.com/uploads/productResources/na/SMART-Stent-with-Stats-Brochure-FINAL.pdf⟩ (accessed May 20, 2024).
[139] InnovaTM Vascular Self-Expanding Stent System - Boston Scientific, (2024). ⟨https://www.bostonscientific.com/en-US/products/stents–vascular/Innova_Vascular_Self-Expanding_Stent_System.html⟩ (accessed May 17, 2024).
[140] Supera Peripheral Stent System | Abbott, (2024). ⟨https://www.cardiovascular.abbott/int/en/hcp/products/peripheral-intervention/supera-stent-system/overview.html⟩ (accessed May 17, 2024).
[141] Absolute Pro Vascular Self-Expanding Stent System | Abbott, (2024). ⟨https://www.cardiovascular.abbott/us/en/hcp/products/peripheral-intervention/peripheral-stents/absolute-pro-vascular.html⟩ (accessed May 17, 2024).
[142] EverFlex with Entrust - Peripheral and Billary Stents | Medtronic, (2024). ⟨https://www.medtronic.com/us-en/healthcare-professionals/products/cardiovascular/peripheral-biliary-stents/everflex-entrust.html⟩ (accessed May 17, 2024).
[143] LifeStentTM 5F Vascular Stent System | BD, (2024). ⟨https://www.bd.com/en-us/products-and-solutions/products/product-families/lifestent-5f-vascular-stent-system⟩ (accessed May 17, 2024).
[144] S.M.A.R.T. Vascular Stent Systems, For the Treatment of Superficial Femoral Artery (SFA) or Iliac Lesions (featuring results of the STROLL study), 2024. ⟨https://cordis.com/uploads/productResources/na/SMART-Stent-STROLL-Brochure-Final-2-3-2023.pdf⟩ (accessed May 17, 2024).
[145] M. Lugli, O. Maleti, Preliminary report on a new concept stent prototype designed for venous implant, Phlebology 30 (2014) 462–468, https://doi.org/10.1177/0268355514539680.
[146] E.H. Murphy, Surveying the 2019 venous stent landscape, Endovasc. Today 18 (2019) 53–64.
[147] C. Gopalan, E. Kirk, The blood vessels, Biol. Cardiovasc. Metab. Dis. (2022) 35–51, https://doi.org/10.1016/B978-0-12-823421-1.00004-4.
[148] WALLSTENT Endoprosthesis, Proven Solutions, Dependable Choice, (2012). ⟨https://www.bostonscientific.com/content/dam/bostonscientific/pi/portfolio-group/Stents/WALLSTENT-Endo/Resources/WALLSTENT%20Brochure%20⟩⟨(PI-49409-AB).pdf⟩ (accessed May 17, 2024).
[149] BARD, Instructions for use (IFU) - E-LUMINEXX Vascular Stent, (2008). ⟨https://www.accessdata.fda.gov/cdrh_docs/pdf8/P080007c.pdf⟩ (accessed May 17, 2024).
[150] G. Maleux, P. Gillardin, S. Fieuws, S. Heye, J. Vaninbroukx, K. Nackaerts, Large-bore nitinol stents for malignant superior vena cava syndrome: factors influencing outcome, Am. J. Roentgenol. 201 (2013) 667–674, https://doi.org/10.2214/AJR.12.9582.
[151] optimed - sinus-venous, (2024). ⟨https://assets-global.website-files.com/615ad184f6b9340a65c4de56/6220e4c0aaf85708bd72ffc5_sinus-Venous-9999-0291-07-2018-WEB.pdf⟩ (accessed May 17, 2024).
[152] Sinus obliquus, Stent venoso autoespandibile - Seda Spa, (2024). ⟨https://www.seda-spa.it/sinus-obliquus_8.shtml⟩ (accessed May 17, 2024).
[153] S.M. Shamimi-Noori, T.W.I. Clark, Venous Stents: Current Status and Future Directions, Tech. Vasc. Inter. Radio. 21 (2018) 113–116, https://doi.org/10.1053/J.TVIR.2018.03.007.
[154] T. Mokry, N. Bellemann, C.M. Sommer, C.P. Heussel, F. Bozorgmehr, D. Gnutzmann, N.A. Kortes, H.U. Kauczor, B. Radeleff, U. Stampfl, Retrospective study in 23 patients of the self-expanding sinus-XL stent for treatment of malignant superior vena cava obstruction caused by non–small cell lung cancer, J. Vasc. Interv. Radiol. 26 (2015) 357–365, https://doi.org/10.1016/J.JVIR.2014.11.019.
[155] Sinus-XL 6F, Self-expanding stent for great vessels - Seda Spa - Optimed, (2024). ⟨https://www.seda-spa.it/en/sinus-xl-6f_41.shtml⟩ (accessed May 17, 2024).
[156] Abdominal aorta stent - sinus-XL Flex - OptiMed - descending thoracic aorta / vena cava / nitinol, (2024). ⟨https://www.medicalexpo.com/prod/optimed/product-69605-684434.html⟩ (accessed May 17, 2024).
[157] Sinus-XL Flex, Stent autoespandibile dedicato per i grandi vasi - Optimed, (2024). ⟨https://www.seda-spa.it/sinus-xl-flex_42.shtml⟩ (accessed May 17, 2024).
[158] FDA Summary of Safety and Effectiveness Data (SSED) - Boston Scientific VICI VENOUS STENT System, (2019). ⟨https://www.accessdata.fda.gov/cdrh_docs/pdf18/P180013B.pdf⟩ (accessed May 17, 2024).
[159] M.D. Dake, G. O'Sullivan, N.W. Shammas, M. Lichtenberg, B.P. Mwipatayi, R. A. Settlage, for the V.T. Investigators, three-year results from the venovo venous stent study for the treatment of iliac and femoral vein obstruction, Cardiovasc Interv. Radio. 44 (2021) 1918–1929, https://doi.org/10.1007/s00270-021-02975-2.
[160] Venovo Venous Stent System - 10mm x 60mm x 80cm, (2024). ⟨https://medicalmaterials.com/all-products/venovo-venous-stent-system-10mm-x-60mm/⟩ (accessed May 17, 2024).
[161] ABRE Study A multi-center, non-randomized study to evaluate the safety and effectiveness of the Abre venous self-expanding stent system in patients with symptomatic iliofemoral venous outflow obstruction. Clinical Investigation Plan (CIP), 2018.
[162] FDA Summary of Safety and Effectiveness Data (SSED) - ABRE venous Self-expanding stent system, (2020). ⟨https://www.accessdata.fda.gov/cdrh_docs/pdf20/P200026B.pdf⟩ (accessed May 17, 2024).
[163] Abre Venous Stent - Deep Venous Products | Medtronic, (2024). ⟨https://www.medtronic.com/us-en/healthcare-professionals/products/cardiovascular/deep-venous/abre-venous-stent.html⟩ (accessed May 17, 2024).
[164] E. Avgerinos, H. Jalaie, Progress in the management of early thrombus removal, Phlebolymphology 30 (2023) 118–124.
[165] Sinus-Venous, Stent autoespandibile per il trattamento della patologia venosa periferica - Optimed, (2024). ⟨https://www.seda-spa.it/sinus-venous_28.shtml⟩ (accessed May 17, 2024).
[166] Venous stent - VICI VENOUS STENT® - Veniti, (2024). ⟨https://www.medicalexpo.com/prod/veniti/product-93953-577259.html⟩ (accessed May 20, 2024).
[167] N. Li, R. Al-Hakim, S. Lewis, J. Ferracane, S. Rugonyi, L. Campos, K. Farsad, J. Kaufman, Coaxial placement of balloon-expandable and self-expanding stents: impact on crush resistance and luminal recovery in a benchtop model, J. Vasc. Interv. Radiol. 34 (2023) 1958–1962.e1, https://doi.org/10.1016/J.JVIR.2023.07.003.
[168] M. Hejazi, A Comparative Assessment of Deformation Characteristics of Self-Expanding Venous Stents, Master of Applied Science thesis, The University of British Columbia, 2018.
[169] Zilver Vena® Venous Self-Expanding Stent | Cook Medical, (2024). ⟨https://www.cookmedical.com/products/f3af274c-42cc-42cd-a0db-e5715ad57cc4/⟩ (accessed May 17, 2024).
[170] A.G. Verstandig, A.I. Bloom, T. Sasson, Y.S. Haviv, D. Rubinger, Shortening and migration of wallstents after stenting of central venous stenoses in hemodialysis patients, Cardiovasc Interv. Radio. 26 (2003) 58–64, https://doi.org/10.1007/s00270-002-1953-6.
[171] V. Finazzi, A.G. Demir, C.A. Biffi, C. Chiastra, F. Migliavacca, L. Petrini, B. Previtali, Design rules for producing cardiovascular stents by selective laser melting: geometrical constraints and opportunities, Procedia Struct. Integr. 15 (2019) 16–23, https://doi.org/10.1016/J.PROSTR.2019.07.004.
[172] A. Guerra, A. Roca, J. de Ciurana, A novel 3D additive manufacturing machine to biodegradable stents, Procedia Manuf. 13 (2017) 718–723, https://doi.org/10.1016/J.PROMFG.2017.09.118.
[173] P.P. Selvakumar, M.S. Rafuse, R. Johnson, W. Tan, Applying Principles of Regenerative Medicine to Vascular Stent Development, Front Bioeng Biotechnol 10 (2022). ⟨https://www.frontiersin.org/articles/10.3389/fbioe.2022.826807⟩.
[174] S. Choudhury, S. Asthana, S. Homer-Vanniasinkam, K. Chatterjee, Emerging trends in biliary stents: a materials and manufacturing perspective, Biomater. Sci. 10 (2022) 3716–3729, https://doi.org/10.1039/D2BM00234E.
[175] K. Nakamura, J.H. Keating, E.R. Edelman, Pathology of endovascular stents, Inter. Cardiol. Clin. 5 (2016) 391–403, https://doi.org/10.1016/J.ICCL.2016.02.006.
[176] B. Kumar, R. Rakesh Ram, N. Dahiya, A.A. Gawalkar, Real-world clinical outcomes of indigenous biodegradable polymer drug-eluting stents, Cureus 13 (2021), https://doi.org/10.7759/cureus.17886.
[177] T.R. Yeazel, M.L. Becker, Advancing toward 3D printing of bioresorbable shape memory polymer stents, Biomacromolecules 21 (2020) 3957–3965, https://doi.org/10.1021/acs.biomac.0c01082.
[178] J. Lai, C. Wang, M. Wang, 3D printing in biomedical engineering: processes, materials, and applications, Appl. Phys. Rev. 8 (2021) 021322, https://doi.org/10.1063/5.0024177.
[179] M. Ullah, A. Bibi, A. Wahab, S. Hamayun, M.U. Rehman, S.U. Khan, U.A. Awan, N. ul ain Riaz, M. Naeem, S. Saeed, T. Hussain, Shaping the future of cardiovascular disease by 3D printing applications in stent technology and its clinical outcomes, Curr. Probl. Cardiol. 49 (2024) 102039, https://doi.org/10.1016/J.CPCARDIOL.2023.102039.
[180] M.H. Mobarak, M.A. Islam, N. Hossain, M.Z. Al Mahmud, M.T. Rayhan, N.J. Nishi, M.A. Chowdhury, recent advances of additive manufacturing in implant fabrication – a review, Appl. Surf. Sci. Adv. 18 (2023) 100462, https://doi.org/10.1016/J.APSADV.2023.100462.
[181] F. Garcia-Villen, F. López-Zárraga, C. Viseras, S. Ruiz-Alonso, F. Al-Hakim, I. Diez-Aldama, L. Saenz-del-Burgo, D. Scaini, J.L. Pedraz, Three-dimensional printing as a cutting-edge, versatile and personalizable vascular stent manufacturing procedure: toward tailor-made medical devices, Int J. Bioprint 9 (2022) 219–255, https://doi.org/10.18063/IJB.V9I2.664.

[182] C. Aravena, T.R. Gildea, Patient-specific airway stent using three-dimensional printing: a review, 360-360, Ann. Transl. Med 11 (2023), https://doi.org/10.21037/atm-22-2878.
[183] F. Tang, C. Hu, S. Huang, W. Long, Q. Wang, G. Xu, S. Liu, B. Wang, L. Zhang, L. Li, An innovative customized stent graft manufacture system assisted by three-dimensional printing technology, Ann. Thorac. Surg. 112 (2021) 308–314, https://doi.org/10.1016/J.ATHORACSUR.2020.07.013.
[184] M.-K. Hong, J.-M. Shim, Y.-J. Youn, K.-H. Lee, J.-S. Kim, Y.-G. KO, S.-H. Lee, D. Choi, J. Yoon, Y. JANG, A new stent design for the treatment of true bifurcation lesions: H-side branch stents, J. Inter. Cardiol. 23 (2010) 54–59, https://doi.org/10.1111/j.1540-8183.2009.00519.x.
[185] H. Xue, Z. Luo, T. Brown, S. Beier, Design of Self-Expanding Auxetic Stents Using Topology Optimization, Front Bioeng Biotechnol 8 (2020). ⟨https://www.frontiersin.org/articles/10.3389/fbioe.2020.00736⟩.
[186] M.N. Ali, J.J.C. Busfield, I.U. Rehman, Auxetic oesophageal stents: structure and mechanical properties, J. Mater. Sci. Mater. Med 25 (2014) 527–553, https://doi.org/10.1007/s10856-013-5067-2.
[187] X.L. Ruan, J.J. Li, X.K. Song, H.J. Zhou, W.X. Yuan, W.W. Wu, R. Xia, Mechanical design of antichiral-reentrant hybrid intravascular stent, Int J. Appl. Mech. 10 (2018) 1850105, https://doi.org/10.1142/S1758825118501053.
[188] G. Alaimo, F. Auricchio, M. Conti, M. Zingales, Multi-objective optimization of nitinol stent design, Med Eng. Phys. 47 (2017) 13–24, https://doi.org/10.1016/J.MEDENGPHY.2017.06.026.
[189] D. Carbonaro, F. Mezzadri, N. Ferro, G. De Nisco, A.L. Audenino, D. Gallo, C. Chiastra, U. Morbiducci, S. Perotto, Design of innovative self-expandable femoral stents using inverse homogenization topology optimization, Comput. Methods Appl. Mech. Eng. 416 (2023) 116288, https://doi.org/10.1016/J.CMA.2023.116288.
[190] FDA Summary of Safety and Effectiveness Data (SSED) - BARD E-LUMINEXX Vascular Stent, (2008). ⟨https://www.accessdata.fda.gov/cdrh_docs/pdf8/p080007b.pdf⟩ (accessed May 17, 2024).
[191] Urgent Field Safety Notice - Urgent Medical Device Recall - VICI and VICI RDSTM Venous Stent Systems, (2021). https://www.moph.gov.lb/userfiles/files/Medical%20Devices/Medical%20Devices%20Recalls%202021/20-04-2021/VICIandVICIRDSVenousStent.pdf (accessed May 17, 2024).